BMC Chemistry

RESEARCH

Open Access

Investigation of thermal properties and structural characterization of novel boron-containing Schiff base polymers

Dilek ÇANAKÇI[1*]

Abstract

Three novel Schiff base polymers were synthesized by using the Schiff base monomer obtained using aldehyde containing boric acid and amines containing hydroxyl groups as the starting materials. The polymers were synthesized at the same temperature and using the same amount of oxidizing agent by the oxidative polycondensation method. The characterization of all polymers and monomers was achieved by using Fourier transform infrared spectroscopy (FT-IR), ultraviolet–visible spectroscopy (UV–vis), nuclear magnetic resonance spectroscopy (^{1}H-NMR), liquid chromatography-mass spectrometry (LC–MS), gel permeation chromatography (GPC) and scanning electron microscopy (SEM). The thermal stability of these compounds was studied by employing thermogravimetric analysis (TGA), and thermodynamics parameters such as activation energy (E_a), enthalpy (ΔH), entropy (ΔS), and Gibbs free energy(ΔG) for the decomposition process were calculated using the Flynn–Wall–Ozawa method.

Keywords Schiff base polymer, Thermal stability, Thermodynamics parameters, Characterization

Introduction

Polymers are long-chain, high-molecular-weight compounds that are formed from multiple same or different atomic groups with chemical bonds with various degrees of regular structure. Each polymer chain is connected to other neighboring chains with Van der Waals interactions. This bond creates a much weaker attraction in comparison to covalent bonds. With the help of this interaction, every chain is intertwined in the form of a coil in the melt and constitutes the macroscopic polymer structure. The type of the monomer forming the polymer, the presence of side groups on the polymer chain and the interactions of these structures affect the chemical, physical and mechanical properties of the polymer. Polymers are found in numerous structures on products that we use today. The new monomer that was used for polymer synthesis in this study was a Schiff base monomer. Schiff bases are known as having good nitrogen donor ligands (> C=N–). These Schiff base ligands provide the metal ion with one or more electron pairs during the formation of the coordination compound. Due to these properties that they have, Schiff bases are considered a very important organic class. Schiff bases and transition metal complexes have a wide variety of applications in many fields including analytical, biological and inorganic chemistry. Since Schiff base monomers have very good biological activity, they are used as anticancer [1, 2], antimicrobial [3, 4], antioxidant [5], analgesic [6–9], anti-inflammatory [10], anticonvulsant [11], antituberculosis [12] and anthelmintic [13] agents in the medical field. Schiff bases are also used in many applications as a catalyst, dye, pigment, polymer stabilizer and intermediates in synthesis [14].

In this study aldehydes containing boric acid in their structure were used in the synthesis of the Schiff bases.

*Correspondence:
Dilek ÇANAKÇI
canakcidilek@adiyaman.edu.tr
[1] Vocational School of Technical Sciences, Adıyaman University, Adıyaman 02040, Turkey

Nowadays, boric acid and many compounds containing boric acid as a functional group are used in various industrial fields. For example, boric acid is used in glass production to produce specialized glasses and glass fibers as it increases the resistance of the glass against heat, chemicals and mechanical effects. It may be added to soaps and detergents due to its water softening and antimicrobial properties. It is also used as a binder in ceramic production. In recent years, boronic acid functionalized materials have been developed for selective separation [15]. For example, enrichment of glycoproteins with boric acid has led to the synthesis of new compounds, such as affinity chromatography materials [16, 17], magnetic beads [18, 19], nanoparticles [20] microplates [21, 22] and mesoporous materials [23, 24]. Other areas where boric acid is used are the medicine, agriculture and petrochemical industries [15].

Today, there are many polymers containing different functional groups in their structure. Among these polymers, polymers containing the element B synthesized using the oxidative polycondensation method are very few. In order to reduce this deficiency, an aldehyde containing B in its structure was used in our monomer synthesis stage. Three novel Schiff bases containing boric acid in their structures and three novel polymers by using these Schiff base monomers were synthesized in this study. The synthesized Schiff base monomers and polymers were extensively characterized to obtain information on their physical, chemical and morphological properties. To investigate their thermal stability, in particular, thermogravimetric analyses were conducted at three different heating rates. The obtained data were examined by using the Flynn–Wall–Ozawa method, and the thermodynamic parameters of the compounds during their decomposition reactions were determined.

Experimental

Materials and measurements

3-Formyl-4-methoxyphenylboronic acid, 4-aminophenol, 2-amino-5-methylphenol, 2-amino-4-chlorophenol, hydrochloric acid, ethanol and tetrahydrofuran (THF) were used for the Schiff base monomers synthesis. Potassium hydroxide and sodium hypochlorite were used for the Schiff base polymers synthesis. The solvents used in the absorption analysis of the synthesized compounds were dimethyl sulfoxide (DMSO), ethanol and 1, 4-dioxane (All chemical obtained were from Merck & Country).

The FT-IR data were obtained by using a Spectrum 100 FT-IR instrument Perkin Elmer. The absorption spectra were recorded in three solvents at different polarities on a Lambda 35 ES UV/Vis Spectrophotometer Perkin Elmer, where the scan range was 200–700 nm. The ^{1}H NMR spectra were recorded with an Avance II 400 M NMR spectrometer Bruker at ambient temperature, and tetramethyl silane (TMS) was used as the internal standard (DMSO-d_6 was used as solvent). Mass spectrometry was performed using an LC/MS-TOF Spectrometer Agilent. The molecular weights of the obtained polymers were analyzed using a VISCOTEK 270 max GPC/SEC System Malvern at a 1 mL/min THF flow rate. The morphology and grain size of all materials, as well as their elemental compositions, were examined using a JSM-6510 Series Scanning Electron Microscope. Thermogravimetric analyses (TGA) were carried out on a DTG 60H-DSC 60 Shimadzu device under N_2 gas flow for 5, 15, 45 °C/min at 20–1000 °C.

Synthesis of compounds

Synthesis of the Schiff base monomer

The reaction for Schiff base monomer synthesis was standardized according to the following procedure: 2 mmol of 3-formyl-4-methoxyphenylboronic acid (0.358 g) was dissolved in 20 mL of ethanol and 0.1 mL of HCl in a flask. To this solution was added the amino compound [4-aminophenol for BS-OH, 2-amino-5-methylphenol for BS-CH_3 or 2-amino-4-chlorophenol for BS-Cl (2 mmol)] dissolved in 10 mL of DMSO, and the reaction mixture was refluxed for 6 h at 80 °C until the color of the solution turned completely orange. At the end of the period the solution in the flask was kept at room temperature for one day and orange-colored crystals were obtained. After the Schiff base crystals were filtered, they were recrystallized using an ethanol/water mixture and air-dried (Fig. 1). The synthesized Schiff base monomers were BS-OH: 3-(((4-hydroxyphenyl) imino)methyl)-4-methoxyphenylboronic acid, BS-CH_3: 3-(((2-hydroxy-4-methylphenyl) imino)methyl)-4-methoxyphenylboronic acid and BS-Cl: 3-(((5-chloro-2-hydroxyphenyl)imino) methyl)-4-methoxyphenylboronic acid.

The BS-OH yield was 60.44% as an orange crystal; LC/MS-TOF (m/z): 271; FT-IR (KBr, ν cm^{-1}): 3323, 3188 (O–H), 3052 (C–H, aromatic), 1639 (C=N), 1603 (C=C, aromatic); UV–visible (DMSO, nm): 260, 355; ^{1}H NMR (400 MHz, dmso) δ 10.35 (s, 1H), 10.26 (s, 1H), 9.18 (s, 1H), 8.64 (s, 1H), 8.15 (s, 1H), 8.05 (s, 1H), 7.64 (s,1H), 7.27 (d, J = 8.5 Hz, 1H), 7.17 (d, J = 18.9 Hz, 1H), 6.95 (d, J = 8.3 Hz, 1H), 6.85 (d, J = 7.8 Hz, 1H), 4.00 (s, 3H).

The BS-Cl yield was 51.86% as an orange crystal; LC/MS-TOF (m/z): 305; FT-IR (KBr, ν cm^{-1}): 3330, 3211 (O–H), 3055, 2885 (C–H, aromatic), 1645 (C=N), 1602 (C=C, aromatic); UV–visible (DMSO, nm): 231, 296; ^{1}H NMR (600 MHz, dmso) δ 11.06 (s, 1H), 10.35 (s, 1H), 9.11 (s, 1H), 8.54 (s, 1H), 8.16 (s, 1H), 8.04 (s, 1H), 7.41 (s, 1H), 7.22 (s, 1H), 7.18 (s, 1H), 7.06 (s, 1H), 3.96 (s, 3H).

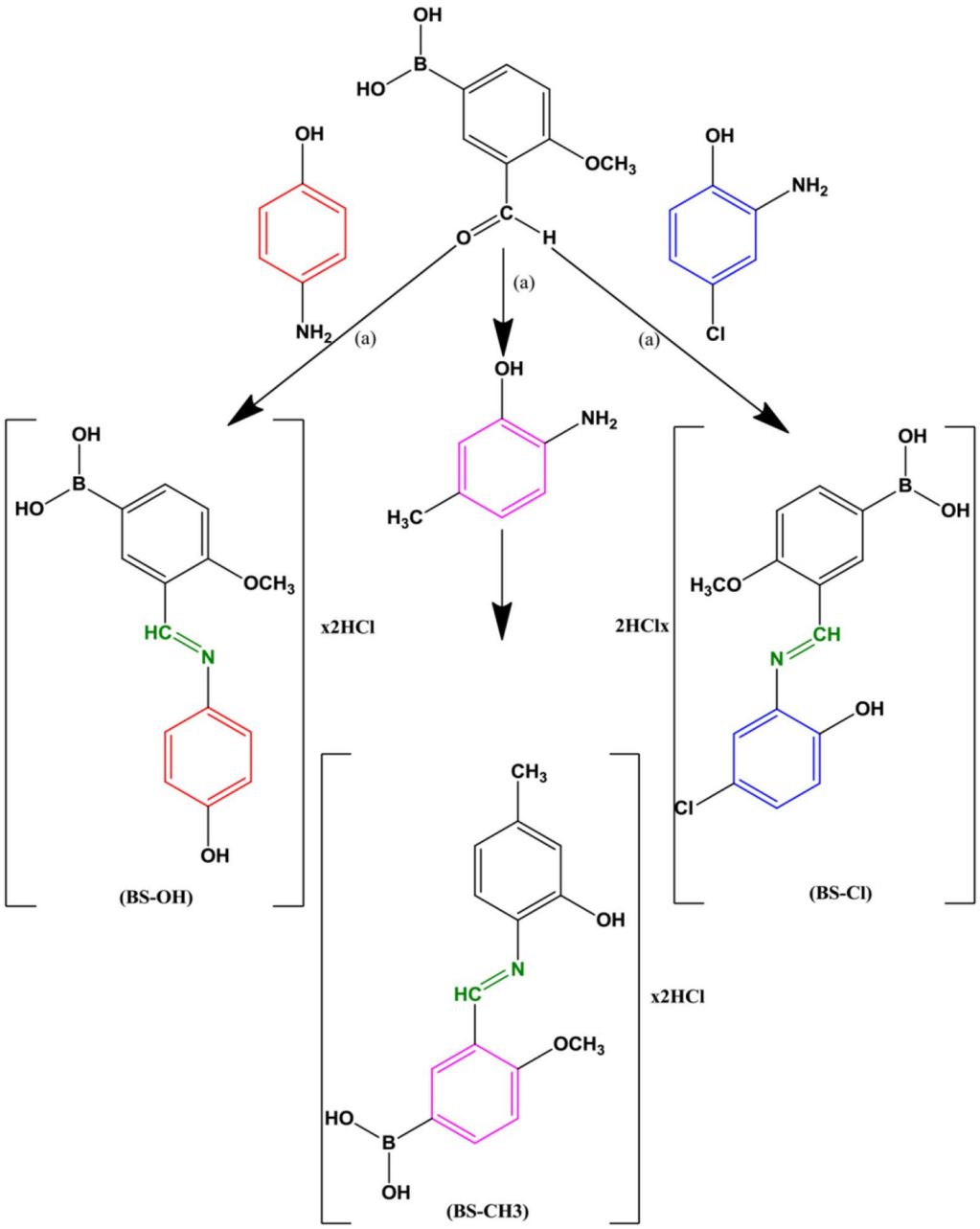

Fig. 1 Preparation of Schiff base monomers (BS-OH, BS-CH_3 and BS-Cl, a; DMSO, ethanol, HCl reflux at 80 °C for 6 h

The BS-CH_3 yield was 61.21% as an orange crystal; LC/MS-TOF (m/z): 286; FT-IR (KBr, ν cm^{-1}): 3322, 3188 (O–H), 3052 (C–H, aromatic), 1639 (C=N), 1600 (C=C, aromatic); UV–visible (DMSO, nm): 224, 263, 359; ^{1}H NMR (600 MHz, dmso) δ 10.61 (s, 1H), 10.35 (s, 1H), 9.76 (s, 1H), 8.57 (s, 1H), 8.16 (s, 1H), 8.05 (s, 1H), 7.18 (d, J = 11.4 Hz, 1H), 6.82 (s, 1H), 6.67 (s, 1H), 3.91 (s, 1H).

Synthesis of the Schiff base polymer

All three novel Schiff base polymers were synthesized by a method reported by us in the literature [25]. After placing 1 mmol of the monomer in a flask, 10 mL of KOH solution (2 mol/L) was added. The mixture was stirred under reflux for 30 min at 70 °C until a homogeneous solution was obtained. After obtaining a clear appearance, 1.2 mL of NaOCl (0.12 mol) was added to

the solution, the temperature was raised to 95 °C and the solution was stirred at this temperature for 8 h. At the end of this period, HCl (37%, 0.5 ml, 0.04 mol) was added to the solution to terminate the polymerization process. The formed polymers were separated from the liquid phase by filtration. The polymers that were obtained were washed with benzene to remove unpolymerized monomers remaining in the structure, and then dried in an oven at 105 °C (Fig. 2). The obtained polymer was purified twice from ethanol/water. The synthesized Schiff base polymers were PBS-OH: poly-(3-(((4-hydroxyphenyl) imino)methyl)-4-methoxyphenylboronic acid), PBS-Cl: poly-(3-(((2-hydroxy-4-methylphenyl)imino)methyl)-4-methoxyphenyl boronic acid) and PBS-CH_3: poly-(3-(((5-chloro-2-hydroxyphenyl)imino)methyl)-4-methoxyphenylboronic acid).

The PBS-OH yield was 59.52% as a black powder; FT-IR (KBr, ν cm^{-1}): 3331, 3231 (O–H), 2887 (C–H, aromatic), 1645 (C=N), 1607 (C=C, aromatic); UV–visible (DMSO, nm): 247, 270, 518; ^{1}H NMR (400 MHz, dmso) δ 10.27 (s, 20H), 10.07 (s, 8H), 9.83 (s, 9H), 9.39 (s, 11H), 9.09–7.67 (m, 197H), 7.44 (s, 11H), 7.27 (s, 15H), 7.13 (s, 15H), 7.07 (dd, J = 26.7, 11.6 Hz, 74H), 6.98 (s, 16H), 6.88 (d, J = 8.7 Hz, 31H), 6.72 (s, 21H), 5.21 (d, J = 1674.3 Hz, 41H), 3.75 (s, 10H), 3.64–3.08 (m, 73H).

The PBS-Cl yield was 54.37% as a black powder; FT-IR (KBr, ν cm^{-1}): 3238 (O–H and C–H, aromatic), 1649 (C=N), 1583 (C=C, aromatic); UV–visible (DMSO, nm): 220, 255, 573; ^{1}H NMR (400 MHz, dmso) δ 10.76 (s, 16H), 10.29–8.02 (m, 21H), 8.44 (s, 13H), 7.24 (d, J = 18.1 Hz, 10H), 7.06 (t, J = 16.3 Hz, 3H), 6.94 (s, 10H), 6.90 (s, 10H), 6.44 (dd, J = 28.8, 13.3 Hz, 2H), 5.08–2.36 (m, 101H).

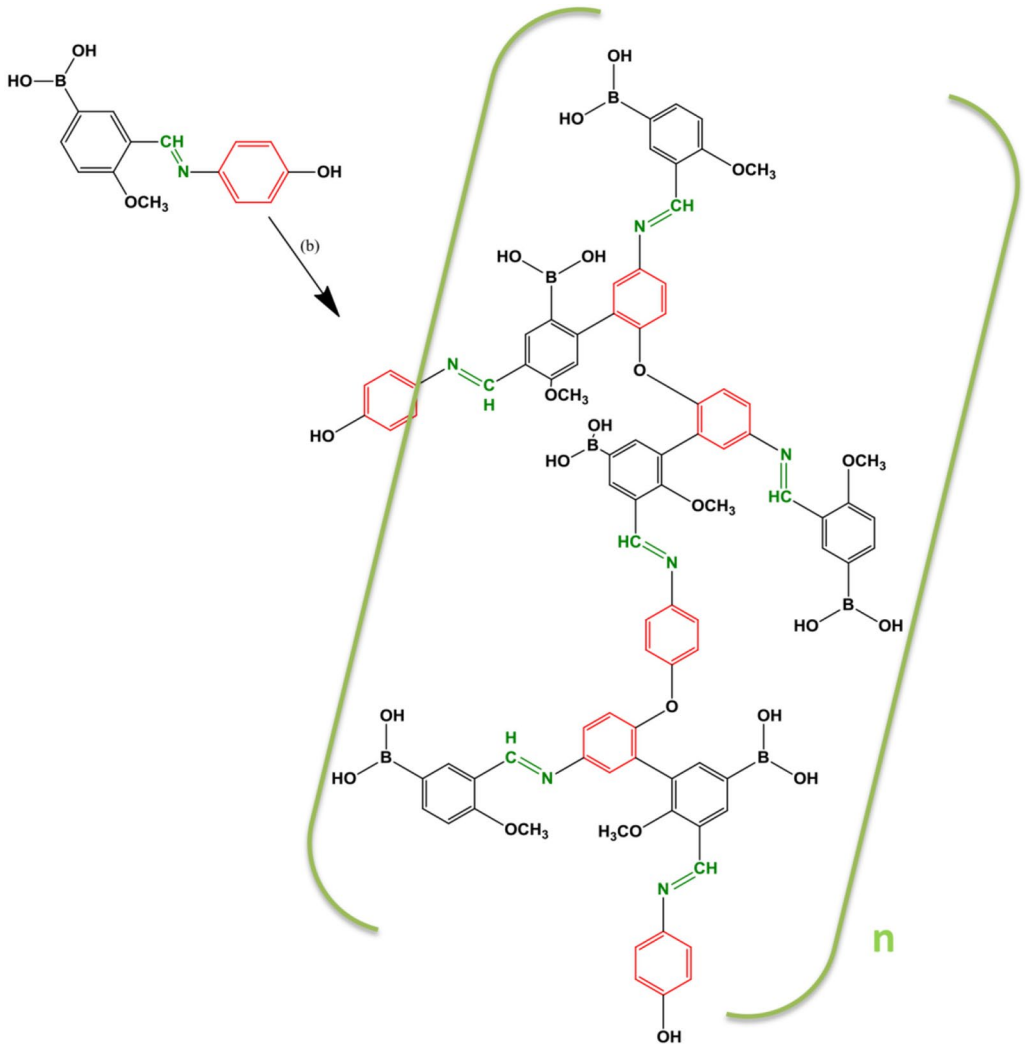

Fig. 2 Preparation of the Schiff base polymer PBS-OH with a polycondensation reaction (b) KOH solution, NaOCl, 95 °C, 8 h

The PBS-CH_3 yield was 36.48% as a black powder; FT-IR (KBr, ν cm^{-1}): 3239 (O–H and C–H, aromatic), 1643 (C=N), 1615 (C=C, aromatic); UV–visible (DMSO, nm): 241, 299; ^{1}H NMR (400 MHz, dmso) δ 10.27 (s, 5H), 9.39 (s, 5H), 7.53 (d, J = 10.3 Hz, 5H), 7.05 (d, J = 14.6 Hz, 20H), 7.00 (s, 5H), 6.93 (dd, J = 29.8, 16.2 Hz, 22H), 6.79 (s, 7H), 6.74 (s, 8H), 6.68 (s, 7H), 6.61 (s, 7H), 6.35 (d, J = 13.2 Hz, 6H), 3.81 (s, 19H), 3.76 (d, J = 15.7 Hz, 17H), 3.70 (s, 11H), 3.36 (s, 464H).

Results and discussion

LC/MS analysis

A LC/MS analysis method was used to determine the molecular weights of the Schiff base monomers. The obtained analysis data showed that a large number of peaks were formed. According to the LC/MS spectra, the molecular ion values (m/z) for BS-OH, BS-Cl and BS-CH_3 were determined to be 271, 305 and 286 (Fig. 3), respectively. Other peaks in the spectrum were formed as a result of the separation of elements from the monomers during ionization. The first group to leave the structure of monomers was HCl bound to the schiff base structure. Then the hydroxyl groups, methyl and chlorine groups were separated from the structure, respectively. In the last step, the structure of the benzene rings was destroyed as a result of ionization. Degraded parts combined between each other and formed compounds having greater molecular weights. This situation caused to be seen more peaks in the LC/MS spectra than expected.

GPC analysis

Polymers chains usually consist of the several different types of atoms that are covalently bonded to each other. Each chain is connected to the other chains by Van der Waals interactions, which create much lower forces of attraction compared to the covalent bonds. Thanks to this interaction, each chain is intertwined with each other coil, forming a macroscopic polymer structure. The molecular weight and distribution of the polymer are important for its chemical and physical properties. Gel permeation chromatography was used to determine the molecular weights of the synthesized polymers. The data obtained showed that the molecular weights (Mn and Mw, g/mol) for PBS-OH were 4.832 and 6.040, for PBS-Cl were 4.911 and 7.220, for PBS-CH_3 were 5.209 and 6.825, respectively. The polydispersity index (PDI) values of the polymers indicated that about 20–25 monomers were involved in the polymerization of each chain (PDI: 1.25 for PBS-OH, 1.47 for PBS-Cl and 1.31 for PBS-CH_3). That the polydispersity index was greater than one shows that, although the repeated monomer units of

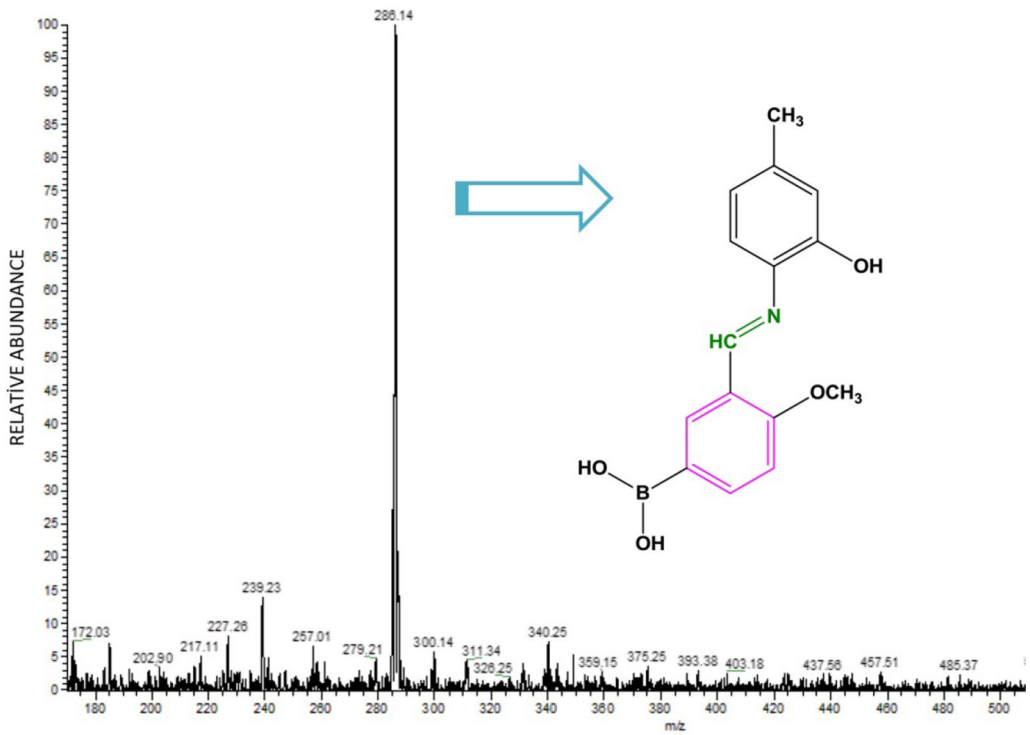

Fig. 3 The liquid chromatography-mass spectrometry (LC/MS) chromatograph of monomer BS-CH_3

each polymer were the same, they were heterogeneous in terms of chain length.

FT-IR analysis

Important characteristic peaks of the synthesized compounds were seen in the IR spectra of the Schiff base monomers and polymers (Figs. 4 and 5, respectively) Stretching vibration peaks, which prove the existence of -OH groups both attached to the benzene ring and in the structure of boronic acid, were observed in the monomer spectra at 3323–3188 cm^{-1} for BS-OH, 3330–3231 cm^{-1} for BS-Cl and 3323–3188 cm^{-1} for BS-CH_3 [26–29]. The medium broad absorption peak observed at 3052 cm^{-1} in the spectrum of BS-OH was assigned to the aromatic C–H stretching vibration. In the BS-Cl and BS-CH_3 spectra, this peak was formed more broadly, respectively, at 3035–2885 and 3052 cm^{-1}. This was because the types of groups attached to the benzene ring and the locations to which they were attached were contradicts. This difference affected the position of the peaks caused by the vibrations of the other groups in the same way.

Even if the main structure of the monomers was the same, the differentiation of the groups in the benzene ring increased or decreased the peak intensities as expected. The strong absorption band observed at 1639 cm^{-1} in the spectrum of BS-OH was assigned to the C=N of the azomethine groups stretching vibrations, indicating the formation of the Schiff base monomer, and the peak at 1379 cm^{-1} was attributed to the C–N stretching vibration [30]. Moreover, the strong peak at 1603 cm^{-1} was assigned to the aromatic C=C stretching vibration of benzene rings. In the BS-Cl and BS-CH_3 spectra, the stretching vibration peak of azomethine corresponding to Schiff base formation was observed at 1645 and 1639 cm^{-1}, respectively. The C–N stretching vibration peak that supported the expected was a bond formation was 1385 cm^{-1} for BS-Cl and 1373 cm^{-1} for BS-CH_3. The aromatic C=C stretching vibration belonging to the benzene rings forming the main structure of the novel compounds was found at 1602 and 1600 cm^{-1}, respectively, in the BS-Cl and BS-CH_3 FT-IR spectra.

One of the best spectroscopic techniques used to study the microstructure of polymers is FT-IR spectroscopy. The difference between the spectra of the synthesized polymers and the spectra of their monomers may be seen clearly. In the spectra of the polymers, the peaks were broader, and the number of the peaks formed may be lower. This was because polymerization formed a macromolecular structure, and the total number of groups therefore more peaks increased due to the repeating units. At the same time, peaks were formed in similar regions as a result of the vibration of the groups, and the peak appearance widened as a result of the overlap of the peaks.

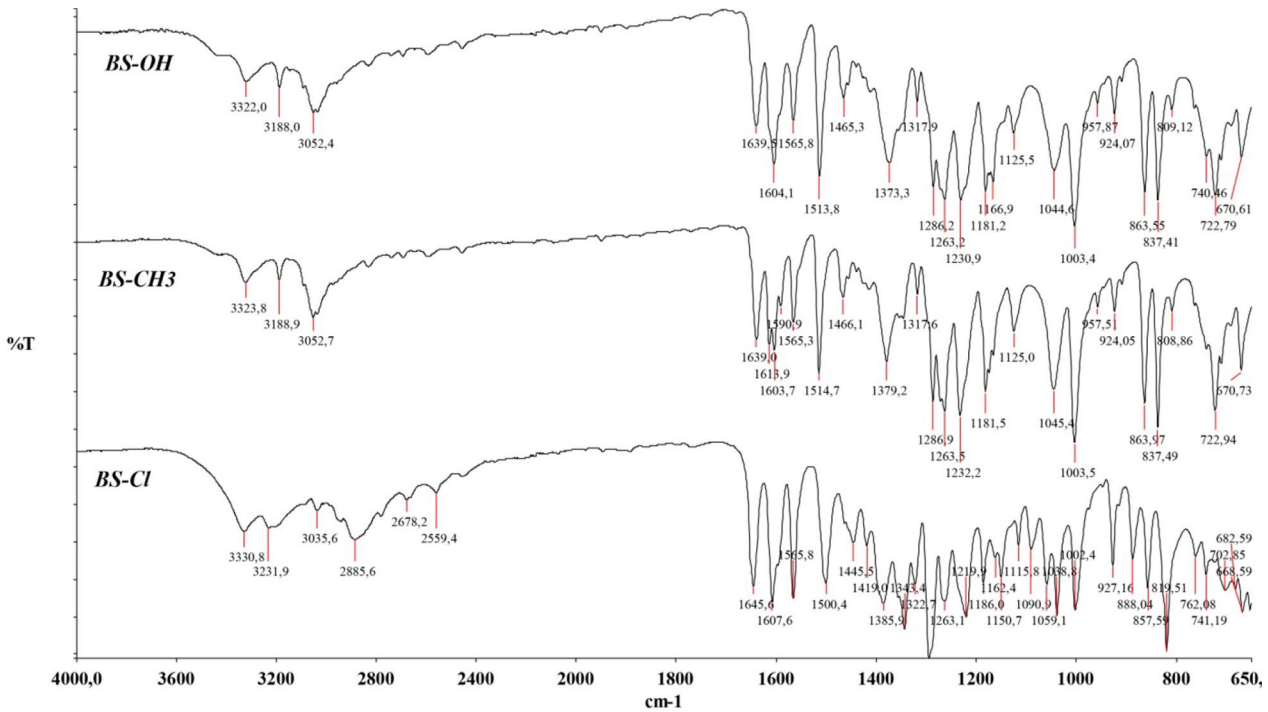

Fig. 4 FT-IR spectrum of Schiff base monomers

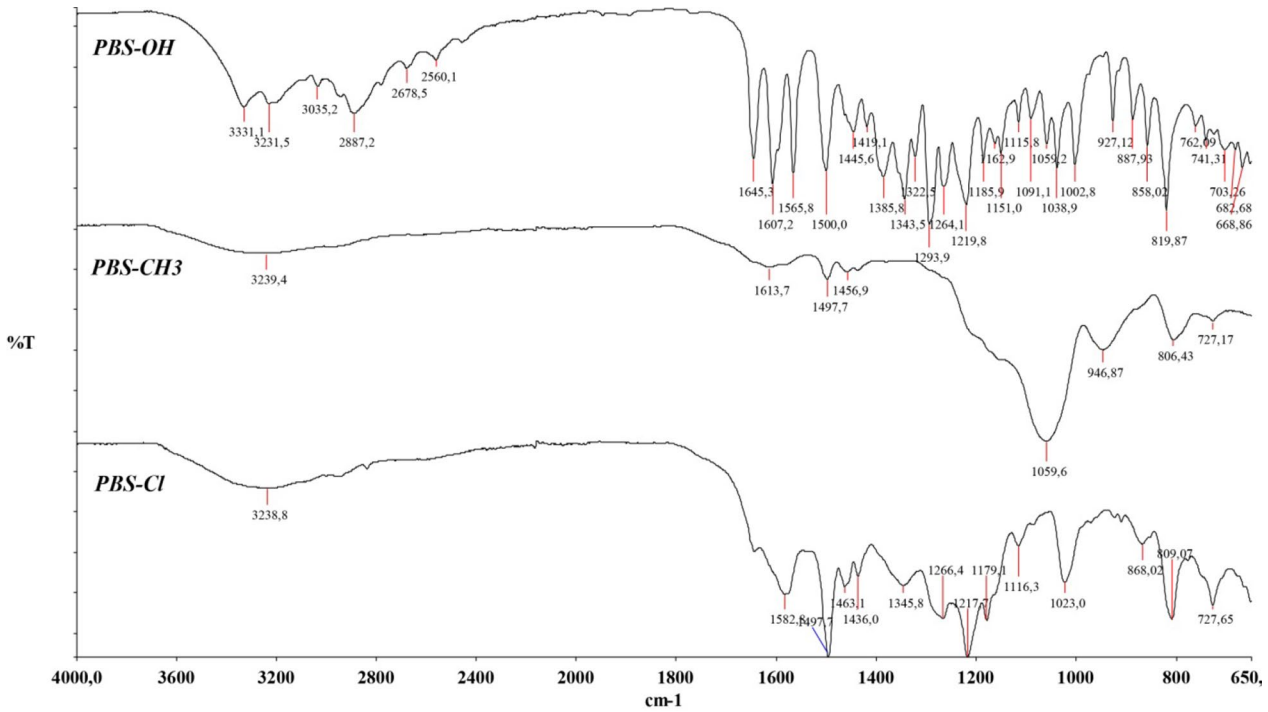

Fig. 5 FT-IR spectrum of Schiff base polymers

In the polymer spectra, it was seen that the –OH and aromatic C–H peaks overlapped and formed quite wide peaks between 2500 cm^{-1} and 3600 cm^{-1}. A similar situation was valid for the C=C and C=N stress vibration peaks, too. These peaks were formed at 1645–1607 cm^{-1} for PBS-OH, 1582 cm^{-1} for PBS-CI and 1613 cm^{-1} for PBS-CH_3 [25].

^{1}H-NMR analysis

The ^{1}H NMR spectra of the novel Schiff base monomers and polymers in DMSO were analyzed with TMS as the standard. The structures of the monomers were characterized from the assignments of the observed chemical shifts to the corresponding protons. The imine proton signal (c in Figs. 6 and 7), proving Schiff base monomer formation, was formed at 8.64 ppm, 8.54 ppm and 8.57 ppm for BS-OH, BS-Cl and BS-CH_3, respectively [31]. The hydroxyl group protons in the structure of the Schiff base monomers generated successive several signals between 9 and 11 ppm. Furthermore, the methoxy proton peaks (d) in the structure were formed at 4 ppm for BS-OH, 3.96 ppm for BS-Cl and 3.91 ppm for BS-CH_3 [32]. The peak observed next to the methoxy proton peak belonged to the water molecule, and the signal observed around 2.5 ppm belonged to the DMSO. Additionally, the presence of aromatic rings was proven by the singlet and doublet signals of aromatic protons between 6.60 and 8.15 ppm.

The ^{1}H NMR spectra of the polymers showed that the polymers were formed. As a result of polymer formation, the number of benzene rings, hydroxyl groups and methoxy protons in the structure increased. So, the same type of proton signals overlapped with each other. All proton signals formed a hill view by generating multiple signals in the regions where they should be. Since polymerization took place over the hydroxyl groups and the benzene rings, the hydroxyl proton signals were lower and did not form a hill view. The hydroxyl proton signals occurred as mostly three singlets for PBS-Cl in the range of 9.68–10.76 ppm. Imine and methoxy proton signals occurred in the spectra between 8.74 and 9.40 ppm and between 3.58 and 3.94 ppm, respectively. The most significant evidence supporting polymer formation in the spectra was the wide hill appearance formed by the overlap of benzene proton peaks in the range of 5.48–8.44 ppm.

SEM and EDX analysis

A scanning electron microscope (SEM) with an Energy Dispersive X-Ray Analyzer (EDX) were used to illuminate the surface morphology of the synthesized Schiff base monomers and polymers and analyze the elemental composition of compounds. The instrument was operated with various magnifications for obtaining the best images

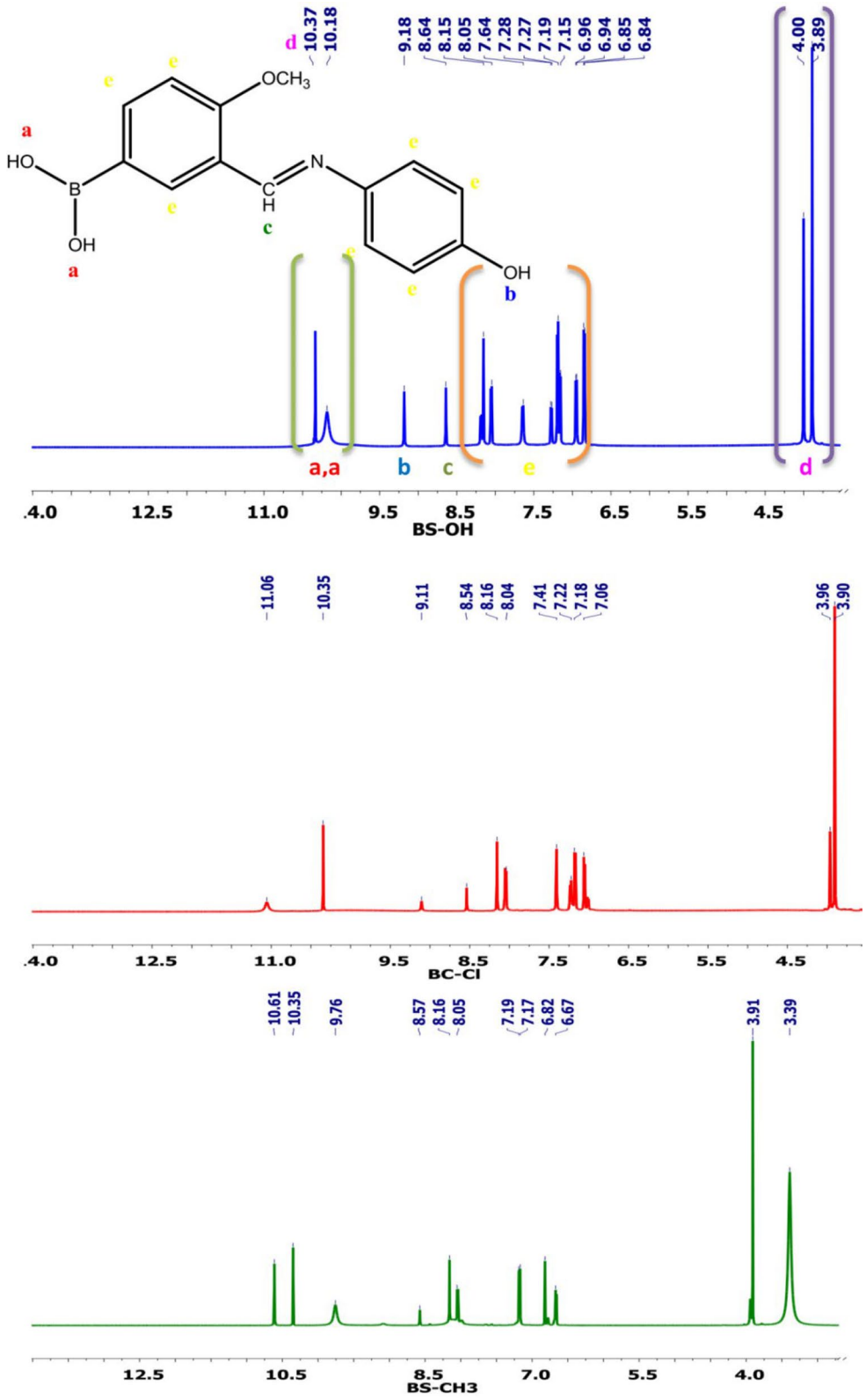

Fig. 6 ^{1}H NMR spectra (400 MHz, dmso) of Schiff base monomers

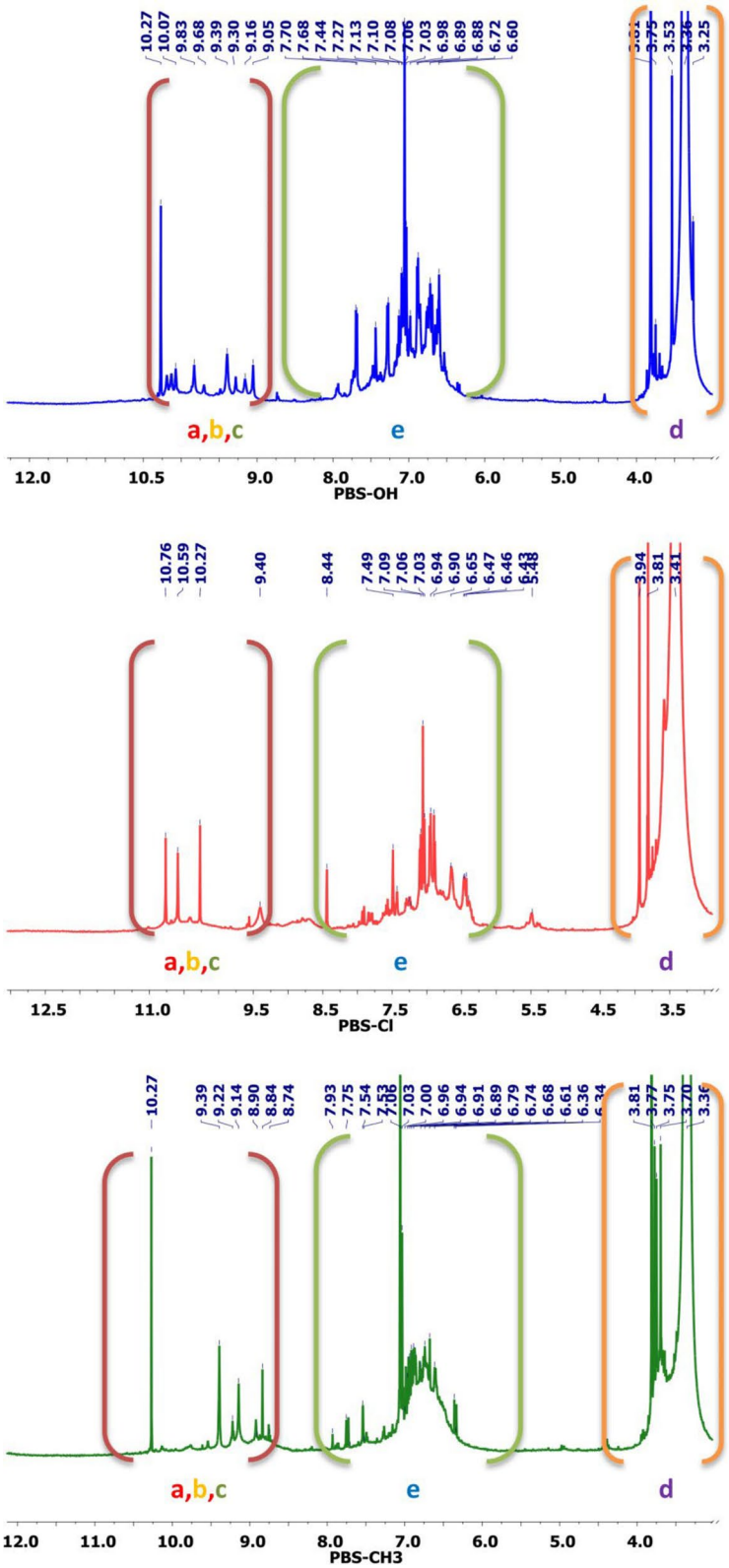

Fig. 7 ^{1}H NMR spectra (400 MHz, dmso) of Schiff base polymers

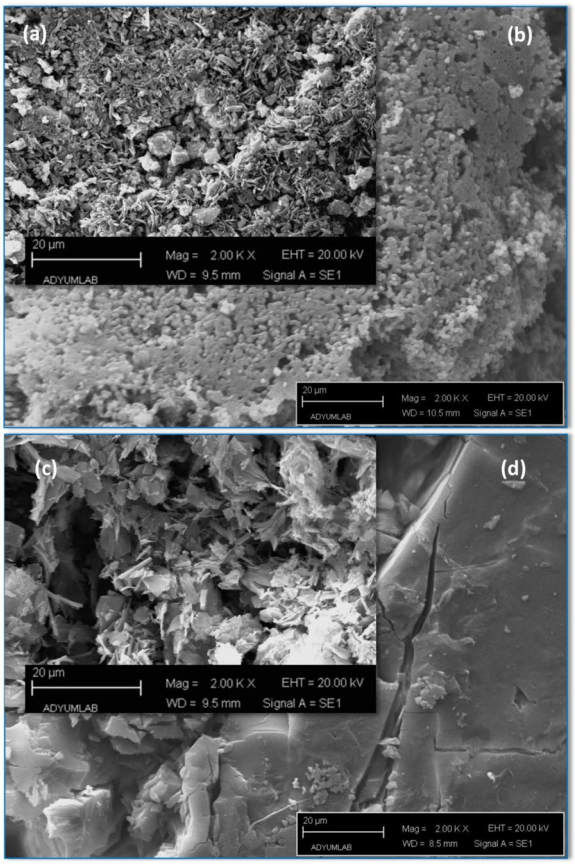

Fig. 8 Scanning electron microscopy (SEM) image of: synthesized compounds: **a** BS-OH; **b** PBS-OH; **c** BS-Cl; **d** PBS-Cl

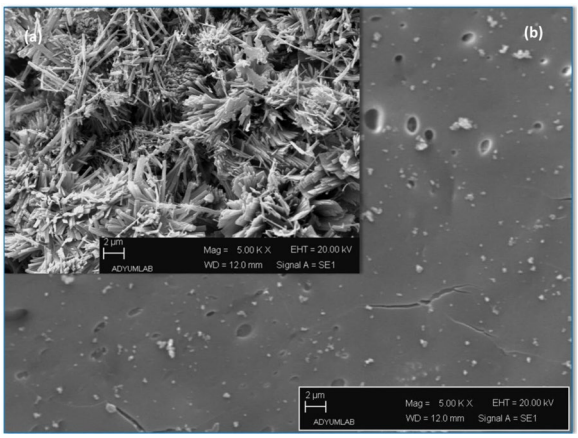

Fig. 9 Scanning electron microscopy (500 KX) image of: the synthesized compounds: **a** BS-CH_3; **b** PBS-CH_3

of the samples (20 kV: 2.00 and 5.00 KX). The SEM images clearly showed that, even if the main chemical structure of the monomers was similar, different groups attached to the benzene ring affected the morphologies of the compounds (Figs. 8 and 9).

Especially when the morphological structure of BS-CH_3 was evaluated in terms of roughness, pore size and geometry parameters, it was seen that it was quite different from BS-OH and BS-Cl. All three monomers had a fibrous structure on their surface, and there were also crystallized particles independent of the matrix structure. However, the surface structure of BS-CH_3 was more stratified than the other two monomers. BS-CH_3 had the most multi- fibrous structure among the monomers, and so its pore size and number were higher than the others. The SEM images obtained at different magnifications proved that the morphology of the Schiff base monomers changed as a result of the polymerization. The biggest difference that can be seen in the SEM images of monomer and polymer is that the monomers lost their fibrous crystal structure as a result of polymerization. In addition, the layer structure and the number of pores monomers decreased. When the SEM images of the polymers were examined in terms of the number of pores, it was seen that the order was in the form of PBS-OH, PBS-Cl and PBS-CH_3 from largest to smallest. All polymers had small particles of various sizes on their surfaces. In particular, SEM images of PBS-CH3 showed a large number of small particles independent of the main structure.

Qualitative and quantitative elemental analysis of the monomers was performed using the Energy Dispersive X-Ray Analysis (EDX) method. The data obtained showed that the monomers contained the expected elements (C, O, N, B) and that HCl was attached to the main structure during Schiff base synthesis. The percentage of Cl in the compounds was about 20% for all three monomers (Fig. 10). This result showed that approximately 2 HCl groups were bound to each of the Schiff base monomers. As a result of polymerization, th HCl, which depends on the structure of the monomer, was separated from the main structure.

UV–vis analysis

UV spectroscopic analysis of the synthesized Schiff base monomers and polymers was performed by using solvents with three different polarities to investigate the electromagnetic beam absorption properties in the UV–vis region. The absorption spectra of the compounds obtained using dimethyl sulfoxide (DMSO), dimethylformamide (DMF) and ethanol solvents are given in Fig. 11. All spectra showed that the compounds underwent $\pi \rightarrow \pi^*$, $n \rightarrow \pi^*$ and charge-transfer electronic transitions at various wavelengths in the polar protic (DMSO and Ethanol) and polar aprotic (DMF) solvents. The bands seen in the spectra are given in Tables 1 and 2. The Schiff base monomers and polymers formed $\pi \rightarrow \pi^*$ (E_2 and

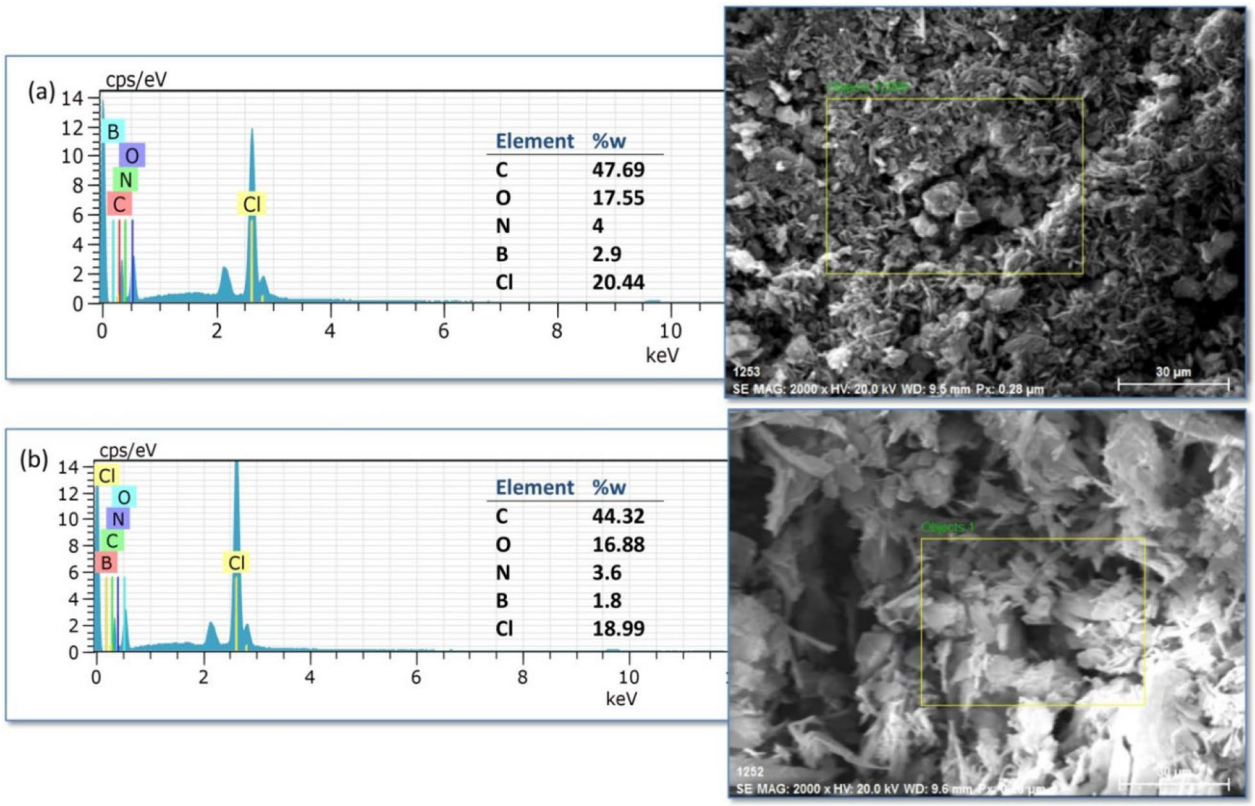

Fig. 10 EDX spectra and SEM image of **a** PBS-Cl and **b** BS-Cl

B band) and n → π * bands due to the benzene rings in their structures. Additionally, BS-Cl and BS-OH formed the charge-transfer transition band in the DMF and DMSO solvents, respectively. When the spectra of the polymers and monomers were compared, it was seen that there was 25 expected shift in the positions of the bands belonging to the electronic transitions. This was because, as a result of polymerization, many benzene rings formed bonds with each other, and this led to the formation of conjugate structures that would allow electronic transitions to occur more easily. The monomers formed bands in the DMF solution in the 226–293 nm range due to π → π * (E_2 band) electronic transitions and in the range of 320–400 due to π → π * (B Band) electronic transitions. Additionally, BS-Cl, unlike the other monomers in DMF solvent, formed a broad band at 572 nm due to the charge-transfer-complex (CTC) transition. This result indicated that the interaction of the BS-Cl monomer with the DMF solvent was different from the other monomers. This band was formed by the excitation of an electron in the monomer structure with a photon and transferring of this electron to the DMF. In this case, only partial charge transfer occurred on the electronic basic level, and this created the CTC transition band. The CTC transfer band was formed between 516 and 576 nm in the spectra of all synthesized polymers.

The CTC transfer band was formed at 554 nm for PBS-OH, 570 nm for PBS-Cl and 576 nm for PBS-CH_3 [33]. The reason why PBS-OH and PBS-CH_3 formed bands in the visible region, different from their monomers, was that the electron density increased due to the presence of numerous benzene rings (electron donors) in the structure of the polymers, and therefore, easier electron transfer to the molecule with less electron density (electron acceptor) was provided. When the spectra of the monomers and polymers in DMSO and ethanol were compared to the spectra in DMF it was clearly seen that there was a shift in the absorption bands. BS-Cl, which formed the CTC band (572 nm) in the DMF, did not form this band in DMSO and ethanol. Additionally, PBS-Cl in DMSO and PBS-CH_3 in both DMSO and ethanol did not form the CTC band. PBS-OH formed bands what close to each other in DMSO and ethanol (DMSO λ: 518 nm, ethanol λ: 516 nm). It may be clearly seen from the data that the energy transition of both the monomers and polymers depended on the polarity of the solvent in which they were dissolved.

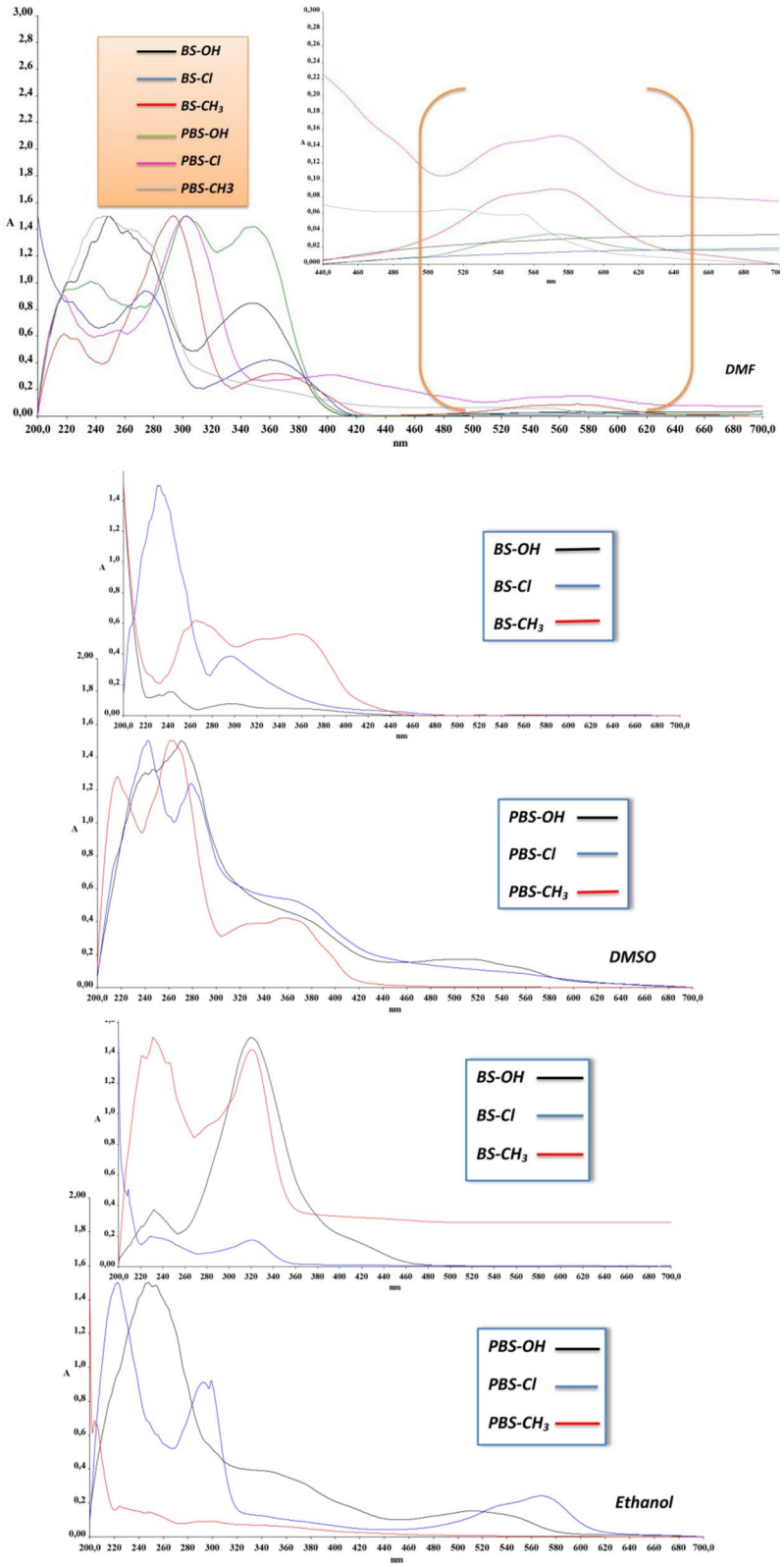

Fig. 11 UV–vis spectra of the Schiff base monomers and polymers in the studied solvents: DMF, DMSO and Ethanol

Thermogravimetric analysis

Thermogravimetric analysis is an analysis method that examines changes in the weight of compounds with temperature. With the method of thermal analysis, changes that occur in the weights of a substance or its derivatives under a temperature program are examined, and the heat absorbed or released in a reaction is measured. To examine the thermal stability levels of the synthesized Schiff base monomers and polymers, TGA/DTA/DTG analyses were carried out at three

Table 1 UV–vis spectrum data of Schiff base monomers in DMF, DMSO and Ethanol

Compound	Solvent	A		B		C		D	
		λ_{max} [a]	ε_{max} [b]	λ_{max} [a]	ε_{max} [b]	λ_{max} [a]	ε_{max} [b]	λ_{max} [a]	ε_{max} [b]
BS-OH	DMF	249	1.49	261	1.38	349	0.84	–	–
	DMSO	–	–	260	0.60	355	0.49	–	–
	Ethanol	232	0.36	–	–	319	1.50	–	–
BS-Cl	DMF	226	0.61	299	1.50	365	0.31	572	0.10
	DMSO	231	1.50	296	0.76	–	–	–	–
	Ethanol	229	1.49	286	1.44	320	0.27	–	–
BS-CH_3	DMF	–	–	274	0.93	360	0.42	–	–
	DMSO	224	1.27	263	1.49	359	0.42	–	–
	Ethanol	231	1.50	–	–	321	1.41	–	–

[a] The wavelength of the band (nm); [b]molar absorptivity coefficient (mol^{-1} l cm^{-1})

Table 2 UV–vis spectrum data of the Schiff base polymers in DMF, DMSO and Ethanol

Compound	Solvent	A		B		C		D	
		λ_{max} [a]	ε_{max} [b]	λ_{max} [a]	ε_{max} [b]	λ_{max} [a]	ε_{max} [b]	λ_{max} [a]	ε_{max} [b]
PBS-OH	DMF	246	1.01	302	1.50	348	1.42	571	0.03
	DMSO	247	1.32	270	1.49	–	–	518	0.17
	Ethanol	247	1.50	253	1.48	345	0.38	516	0.15
PBS-Cl	DMF	236	1.00	302	1.50	349	1.42	570	0.03
	DMSO	220	1.16	255	1.49	–	–	573	0.21
	Ethanol	222	1.50	292	0.92	–	–	567	0.24
PBS-CH_3	DMF	218	0.90	256	0.64	302	0.31	576	0.15
	DMSO	241	0.21	299	0.12	–	–	–	–
	Ethanol	224	0.18	–	–	301	0.09	–	–

[a] The wavelength of the band (nm); [b]molar absorptivity coefficient (mol^{-1} l cm^{-1})

Table 3 Thermal data obtained of monomers by TGA (heating rate β: 5, 15, 45 °C/min.)

Compound	β	T_i	T_{25}	T_{50}	T_{75}	T_f	Residue%
BS-OH	5	128	245	616	762	1000	11.74
	15	140	277	712	–	1000	37.86
	45	154	319	761	–	1000	38.74
BS-Cl	5	97	214	359	719	1000	6.69
	15	123	226	381	539	1000	0.98
	45	137	250	409	599	1000	9.18
BS-CH_3	5	129	163	363	656	1000	15.84
	15	149	218	426	921	1000	23.62
	45	128	265	454	929	1000	21.08

[i] İnitial decomposition temperature, $T_{25, 50, 75}$: temperature for 25, 50, 75% weight loss, [f]end of decomposition

Table 4 Thermal data obtained of polymers by TGA (heating rate β: 5, 15, 45 °C/min.)

Compound	β	T_i	T_{25}	T_{50}	T_{75}	T_f	Residue%
PBS-OH	5	80	338	544	689	1000	2.59
	15	83	374	678	–	1000	29.73
	45	95	391	677	–	1000	42.83
PBS-Cl	5	81	379	714	–	1000	48.44
	15	73	504	847	–	1000	49.40
	45	86	523	932	–	1000	51.92
PBS-CH_3	5	86	347	642	935	1000	26.08
	15	79	397	851	–	1000	46.20
	45	97	428	998	–	1000	53.77

T_i: İnitial decomposition temperature, $T_{25, 50, 75}$: Temperature for 25, 50, 75% weight loss, T_f: end of decomposition experiment

Table 5 Interpretation of the TGA curves recorded at 5, 15 and 45 °C/min.(Schiff base monomers and polymers)

Compound	Step	β_5			β_{15}			β_{45}		
		T_a	T_b	$\%_c$	T_a	T_b	$\%_c$	T_a	T_b	$\%_c$
BS-OH	1st	128–243	212	24.56	14–278	227	24.70	154–318	247	24.98
	2nd	245–1000	664	63.70	279–1000	522	37.44	319–1000	603	36.28
BS-Cl	1st	97–190	167	17.59	123–236	186	22.56	137–277	202	23.75
	2nd	195–405	322	39.46	237–477	386	40.35	276–514	409	44.89
	3rd	409–1000	708	36.26	478–1000	799	36.11	515–1000	809	22.18
BS-CH_3	1st	129–170	148	18.66	149–219	168	19.98	128–265	184	24.86
	2nd	178–427	342	41.52	230–470	409	33.94	267–460	428	27.89
	3rd	430–1000	798	23.98	472–1000	481	22.46	462–1000	488	26.17
PBS-OH	1st	80–388	266	26.54	83–553	143	35.11	96–531	282	32.60
	2nd	390–1000	638	70.87	554–1000	682	35.16	532–1000	702	24.57
PBS-Cl	1st	81–625	381	38.90	73–624	304	27.94	86–666	627	26.73
	2nd	626–1000	774	12.66	626–1000	783	22.66	668–1000	793	21.35
PBS-CH_3	1st	86–552	275	37.30	79–598	297	34.48	97–626	326	33.84
	2nd	554–1000	762	36.62	600–1000	712	19.32	628–1000	686	12.39

T_a: Mass loss temperature ranges, T_b: Maximum temperature on the DTA curve, $\%_c$: Percentage of lost mass of the sample in the temperature range

different heating rates and between 20 and 1000 °C. The obtained results are presented in Tables 3, 4, 5.

In all monomers and polymers, mass loss took place with the increase in temperatures. The reason for this mass loss up to 100 °C was the water absorbed by the compounds. Figure 12 shows the TGA mass loss of the BS-OH monomer at 5, 15 and 45 °C/min heating rate. The thermal decomposition of the monomer took place in two steps at all three heating rates. In the thermal analysis of BS-OH conducted at a rate of 5 °C/min, the decomposition steps occurred as a result of endothermic decompositions in the temperature intervals of 128–243 °C and 245–1000 °C. As a result of the increase in the heating rate, there was a differences in the temperature intervals of the decomposition steps. The temperature differences occurring in the decomposition steps are summarized in Table 5.

While the first step in the thermal analysis conducted at a rate of 15 °C/min occurred in the range of 145–278 °C, the first step range of temperature in the thermal analysis conducted at a rate of 45 °C/min became 154–318 °C. A similar situation was applicable to the second decomposition steps. The second decomposition steps occurred for 15 and 45 °C/min in the respective intervals of 279–1000 °C and 319–1000 °C. It may be clearly seen in the TGA curves of the compounds that the heating rate in the thermal analysis affected the obtained data directly. There was also an increase in the remaining residue amount of the substance in direct proportion to the increase in the heating rate. After the analyses of the BS-OH monomer at the heating rates of 5, 15 and 45 °C/min, the amounts of the residue at 1000 °C were respectively 11.74, 37.86 and 38.74%. The thermal decomposition of BS-Cl occurred in three steps at all applied heating rates, in difference to the case in BS-OH. The starting

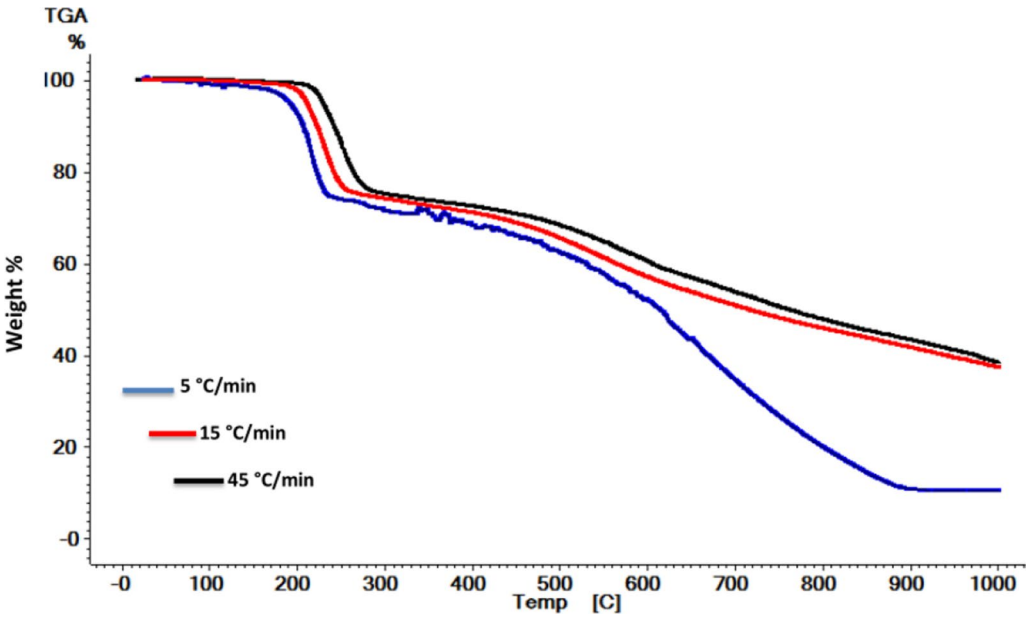

Fig. 12 TGA curves for BS-OH at heating rates of 5, 15, 45 °C/min using an atmosphere of nitrogen at flow rate of 100 mL/min

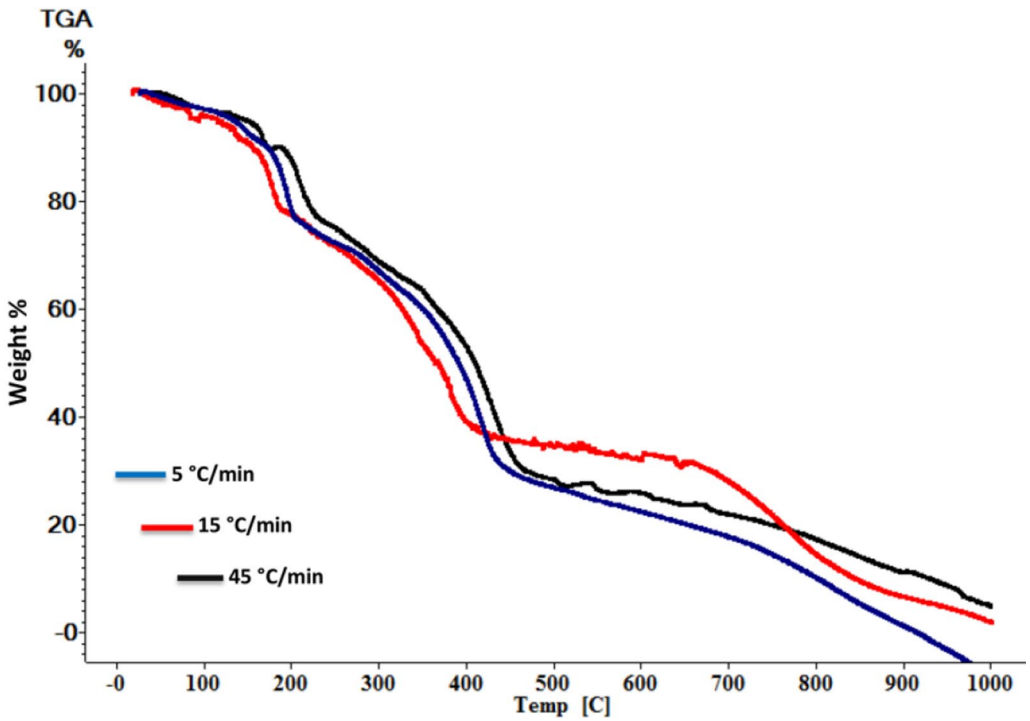

Fig. 13 TGA curves for BS-Cl at heating rates of 5, 15, 45 °C/min using an atmosphere of nitrogen at flow rate of 100 mL/min

temperature of the first decomposition step of BS-Cl was lower than that of BS-OH (Fig. 13). In the analyses of the BS-Cl monomer at the heating rates of 5, 15 and 45 °C/min, the starting temperatures of decomposition were, respectively, 97, 123 and 137 °C. Another difference in the thermal analysis data of BS-OH and BS-Cl was the amount of the remaining residue substance. As a result of the thermal analyzes of BS-Cl, the remaining residue

substance amounts were 6.69%, 0.98% and 9.18% at heating rates of 5, 15 and 45 °C/min, respectively.

The thermal decomposition of the BS-CH_3 monomer also took place in three steps, as in the case of the BS-Cl monomer, (Fig. 14). The decomposition starting temperature of BS-CH_3 was higher than those of both BS-OH and BS-Cl. The decomposition starting temperatures of the monomer at the heating rates of 5, 15 and 45 °C/min were, respectively, 129, 149 and 158 °C. The amount of the remaining substance as a result of the thermal decomposition of the BS-CH_3 monomer was higher than that of BS-Cl and lower than that of BS-OH. After the analyses of the BS-CH_3 monomer conducted at the heating rates of 5, 15 and 45 °C/min, the amounts of the remaining substance were found, respectively, as 15.84, 23.62 and 21.08%.

The data obtained as a result of the thermal analyses of the monomers showed that, although the main structures of the monomers were similar, the fact that the positions and types of the groups connected to the main structure were different affected the monomers' thermal stability directly. Figure 15 shows the TGA curves of the PBS-OH polymer at the 5, 15, 45 °C/min heating rates. As in the case of its monomer, the thermal decomposition of the PBS-OH polymer also took place in two steps.

The TGA data where listed on the all polymers showed that the decomposition starting temperatures of the polymers were lower than those of the monomers. The reason for this was that the ratio of water absorbed by the polymers was higher than that absorbed by the monomers. Moreover, in difference to their monomers, the PBS-Cl and PBS-CH_3 polymers had decompositions in two steps. The first decomposition steps of PBS-OH at the 5, 15, 45 °C/min heating rates took place in the respective temperature intervals of 80–388 °C, 80–553 °C and 96–531 °C. As a result of the thermal analyses, the amounts of remaining substance of PBS-OH at 1000 °C were respectively 2.59, 29.73 and 42.83%. In a similar way to its monomer, the amount of the remaining substances of the polymer increased with increasing heating rate. The amounts of the remaining substance of the PBS-Cl and PBS-CH_3 polymers also were higher than those of both their monomers and the PBS-OH polymer (Figs. 16 and 17). Approximately half of the mass remained undecomposed at all heating rates in the PBS-Cl polymer and at the heating rates of 15 and 45 °C in the PBS-CH_3 polymer. The first reason for this result was that the resistance shown by the polymers against temperature increases were highly different. Although the repeating units of the polymers were the same, the fact that the groups on the units were different changed the characteristic properties of the polymers [33]. –OH and –Cl are electron-donating groups, while –CH_3 is an electron withdrawing group. This difference affected the aromatic structures on the polymer chains and led them to have bonds with different polymer chains, therefore forming a more stable cross

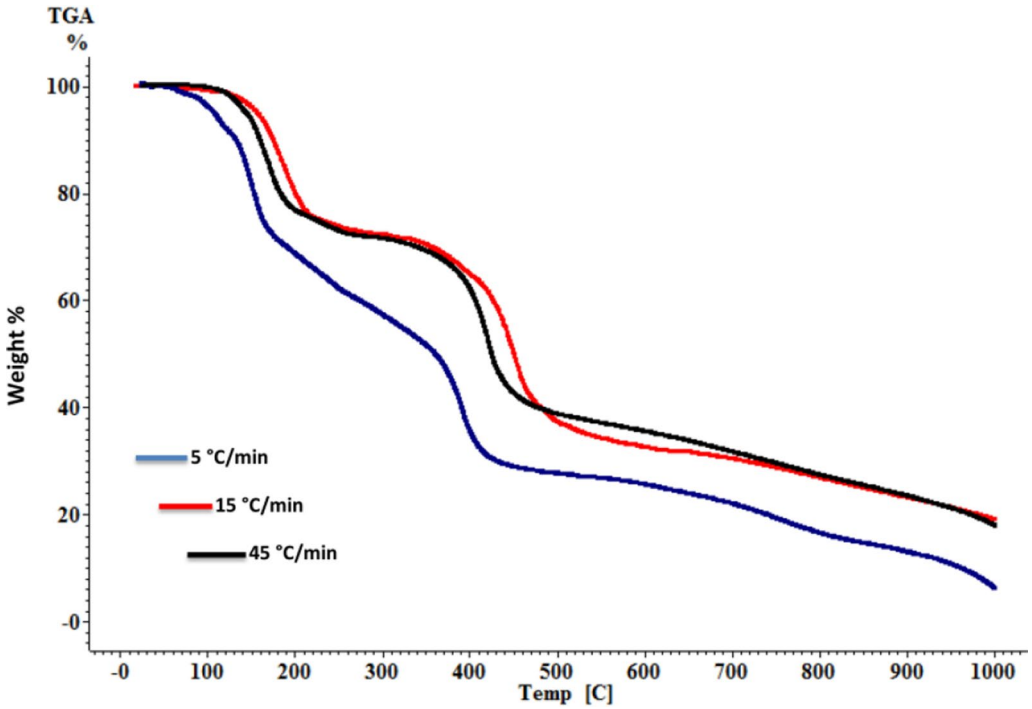

Fig. 14 TGA curves for BS-CH_3 at heating rates of 5, 15, 45 °C/min using an atmosphere of nitrogen at flow rate of 100 mL/min

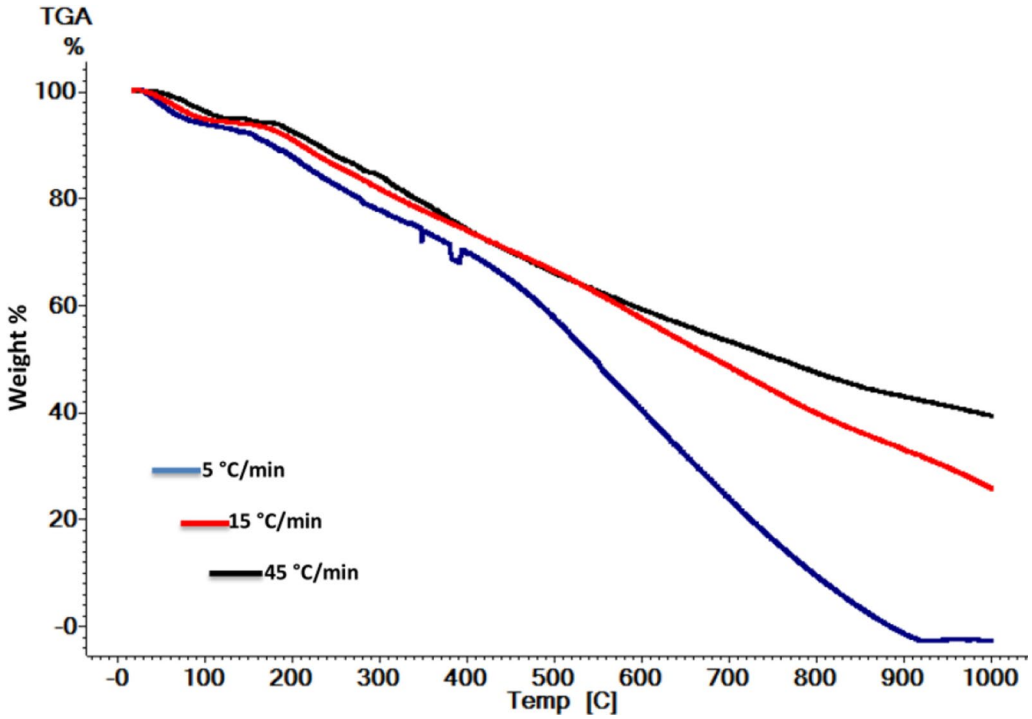

Fig. 15 TGA curves for PBS-OH at heating rates of 5, 15, 45 °C/min using an atmosphere of nitrogen at flow rate of 100 mL/min

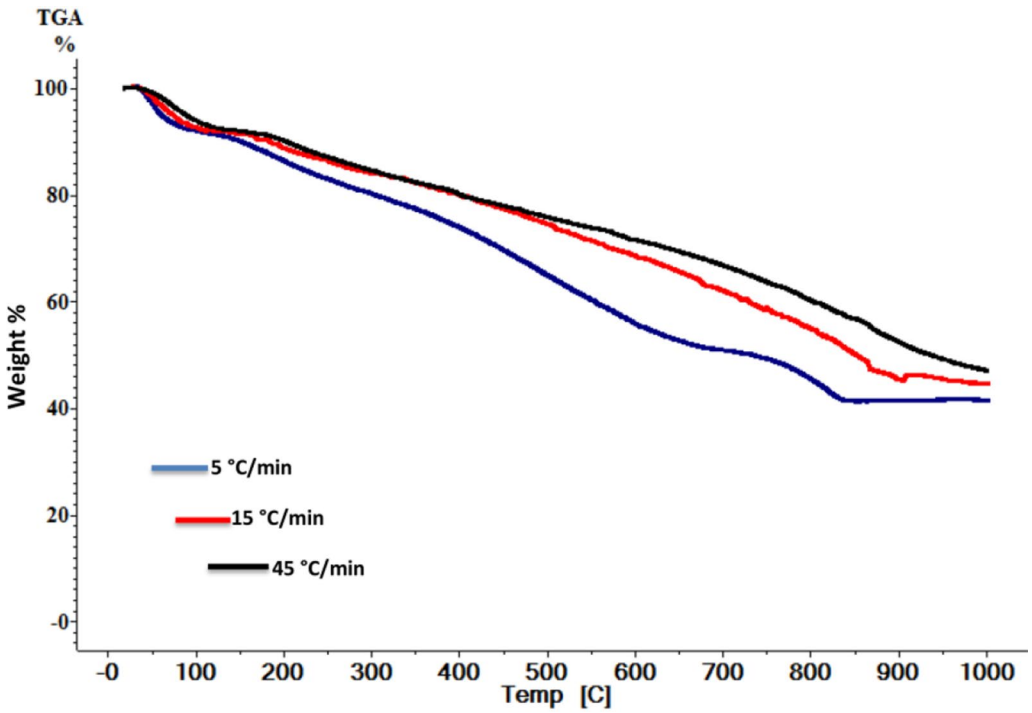

Fig. 16 TGA curves for PBS-Cl at heating rates of 5, 15, 45 °C/min using an atmosphere of nitrogen at flow rate of 100 mL/min

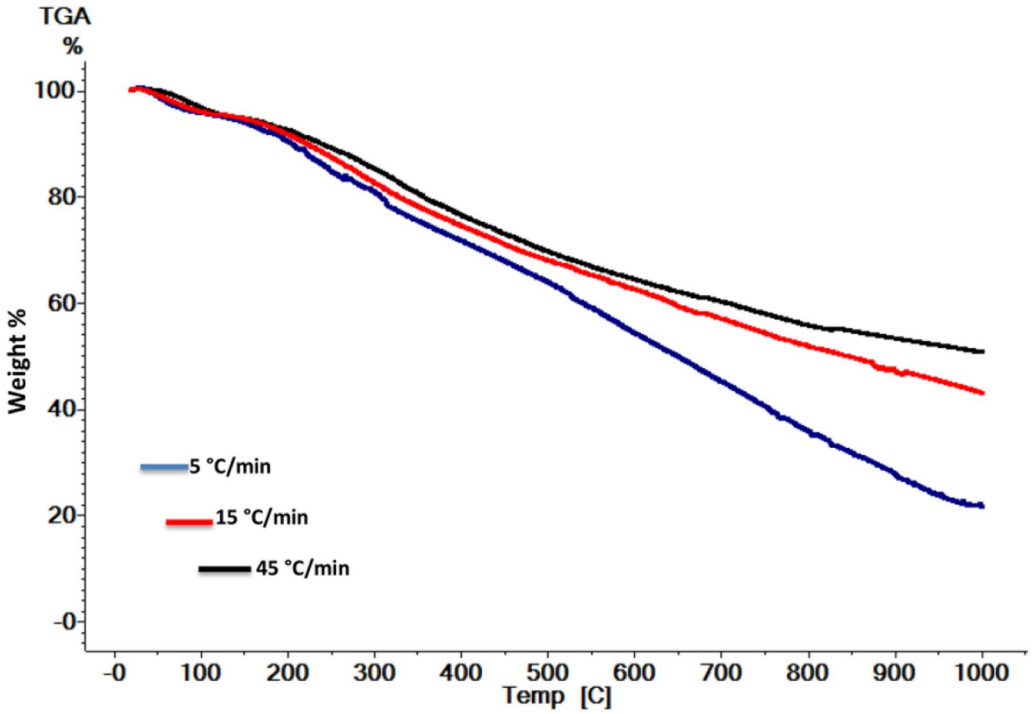

Fig. 17 TGA curves for PBS-CH_3 at heating rates of 5, 15, 45 °C/min using an atmosphere of nitrogen at flow rate of 100 mL/min

linkled structure. As the heat effect influenced the outer layer of the spiral, the inner layers could remain undecomposed. The second reason was the boron compounds forming and remaining in the environment what was as a result of the decomposition of the aromatic structures. Boron is an element with a high thermal resistance and, therefore, the thermal resistance of all compounds it forms is also high.

Kinetic analysis

Based on thermogravimetric findings, several analysis methods have been proposed to obtain information that could be considered significant such as the activation energy and the exponential factor. All kinetic information can be obtained from experiments using different kinetic models. All kinetic studies assume that the isothermal transformation rate, dα/dt, is linearly related to the temperature-related rate constant (k) and the temperature-independent conversion degree (α). That is,

$$\frac{d\alpha}{dt} = k(T)f(\alpha) \tag{1}$$

This expression describes the conversion degree as a function of the reduction in the reactant weight and the rate constant at a constant temperature. According to the Arrhenius equation:

$$k(T) = Aexp\left(-\frac{E_a}{RT}\right) \tag{2}$$

The temperature dependence of the rate consent, k, is expressed in Eq. (2). Therefore, when Eq. (1) is substituted into Eq. (2), Eq. (3) is obtained (A is the exponential factor assumed to be independent of temperature, E is the activation energy, T is the absolute temperature, and R is the gas constant)

$$\frac{d\alpha}{dt} = \mathrm{A}exp\left(\frac{E_a}{RT}\right)f(\alpha) \tag{3}$$

If the sample temperature changes by a controlled and constant heating rate, β = dT/dt, as just β the change in the conversion degree, may be analyzed as a function of the temperature. This temperature is dependent on the heating time. Thus, the transformation rate may be expressed as follows:

$$\frac{d\alpha}{dt} = \beta\frac{d\alpha}{dT} \tag{4}$$

and by combination with the equation above, the following equation is obtained:

$$\frac{d\alpha}{dT} = \frac{A}{\beta}exp\left(\frac{E_a}{RT}\right)f(\alpha) \tag{5}$$

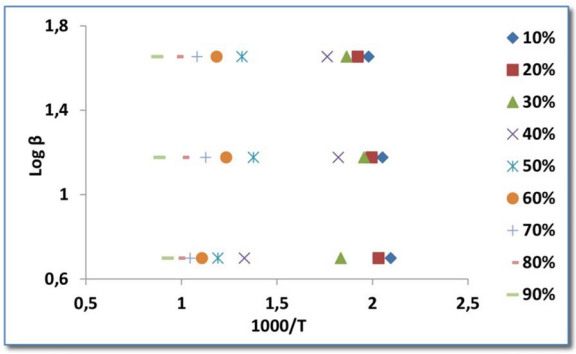

Fig. 18 Ozawa's plots of logarithm of heating rate (Logβ) versus reciprocal temperature (1000/T) at various conversion degrees (%) for BS-OH

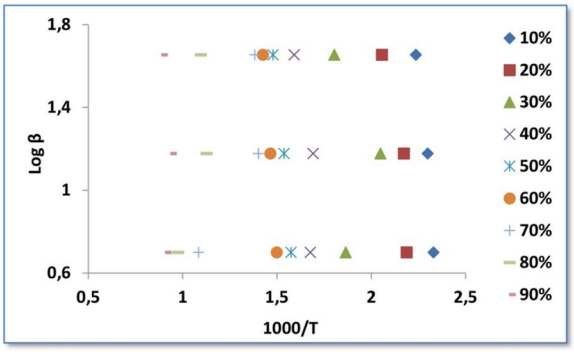

Fig. 19 Ozawa's plots of logarithm of heating rate (Logβ) versus reciprocal temperature (1000/T) at various conversion degrees (%) for BS-Cl

By determining the respective integral limit ranges of 0 and α for the mass transformation fraction values for the thermal reaction start, T_i, and the temperature, T, at any time, the following equation can be written:

$$g(\alpha) = \int_0^{\alpha} \frac{d\alpha}{f(\alpha)} = \frac{A}{\beta} \int_{Ti}^{T} exp\left(\frac{E_a}{RT}\right) dT \tag{6}$$

Here, g(α) is the integral function of the transformation. By applying them in known kinetic methods, these functions are used in the prediction of reaction mechanisms from dynamic TGA curves. New another method, known as the FWO method, which was developed independently by Flynn-Wall and Ozawa to calculate non-isothermal data, is the integral method [34]. Using the Doyle approach and the logarithmic form of Eq. (6), the linear equation of the FWO method is obtained, by transforming the logarithmic expression into the natural logarithm, the following equation is obtained [35].

$$log\beta = log\frac{AE}{Rg(\alpha)} - 2.315 - \frac{0.457.E}{RT} \tag{7}$$

Here β is the heating rate (°C/min). According to this equation, the activation energy can be calculated from the slope in the plot of log β and (1000/T). The slope is equal to the value of '−0.457 E/R'. In this method, as there is a linearity between log β and '1000/T', the curves are parallel to each other for all percentage transformations (Figs. 18, 19, 20, 21, 22, 23).

The activation energies and exponential factors obtained from the plots drawn by using the Flynn–Wall–Ozawa method for all monomers are given in Tables 6, 7, 8 and for all polymers are given in Tables 9, 10, 11.The obtained data showed that the activation energies of the monomers and polymers changed during their thermal degradation process in relation to the transformation percentages (Figs. 24 and 25). As the transformation percentages of the monomers

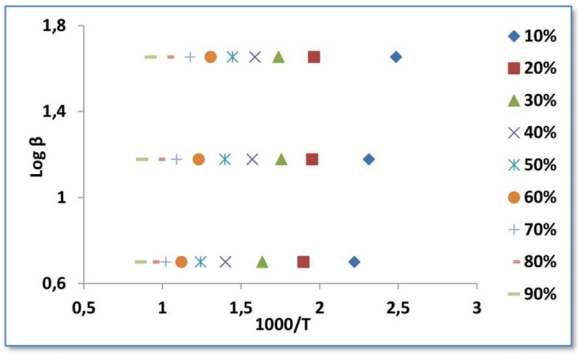

Fig. 20 Ozawa's plots of logarithm of heating rate (Logβ) versus reciprocal temperature (1000/T) at various conversion degrees (%) for BS-CH_3

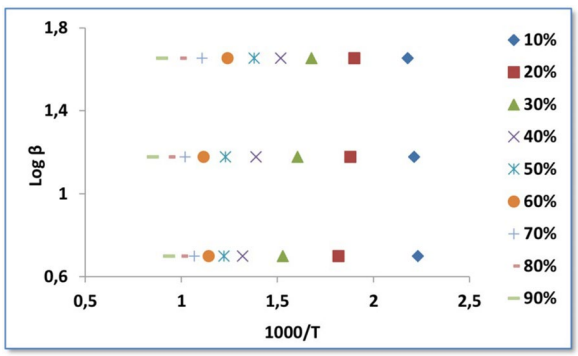

Fig. 21 Ozawa's plots of logarithm of heating rate (Logβ) versus reciprocal temperature (1000/T) at various conversion degrees (%) for PBS-OH

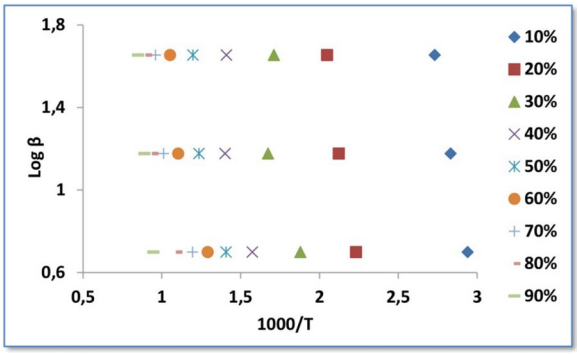

Fig. 22 Ozawa's plots of logarithm of heating rate (Logβ) versus reciprocal temperature (1000/T) at various conversion degrees (%) for PBS-Cl

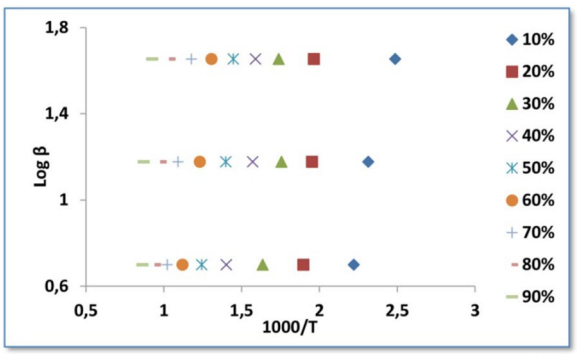

Fig. 23 Ozawa's plots of logarithm of heating rate (Logβ) versus reciprocal temperature (1000/T) at various conversion degrees (%) for PBS-CH_3

and polymers increased, their activation energies also increased. The BS-OH monomer showed the lowest activation energy at the heating rate of 5 °C/min and the transformation percentage of α = 10% (33.28 kJ/mol). When the heating rates were compared by keeping the transformation percentages constant, it was seen that there was mostly an increase in the activation energy. However, the opposite was observed when the transformation percentage was 90%. There was a decrease in the activation energy with the increase in the heating rate. The highest activation energy was obtained at the heating rate of 5 °C/min and the transformation percentage of α = 10% (92.37 kJ/mol). It was observed that the activation energies of BS-Cl and BS-CH_3 were higher in comparison to BS-OH. Especially, BS-CH_3 had a higher activation energy than the other two monomers at all three heating rates. For BS-Cl, the lowest activation energy was obtained at the heating rate of 5 °C/min (α: 10%, E_a: 30 kJ/mol), while the highest one was obtained at the heating rate of 45 °C/min (α: 90%, E_a: 93.20 kJ/mol). For the activation values of BS-CH_3, the highest one was obtained likewise at the heating rate of 45 °C/min (α: 90%, E_a: 94.95 kJ/mol), and the lowest one was at 5 °C/min (α: 10%, E_a: 39.59 kJ/mol).

Considering the activation energies of the polymers, it was observed that these values increased as the transformation percentages increased from 10 to 90%, as in the case of the monomers of these polymers. The highest activation energies were found at the heating rate of 15 °C/min for PBS-OH (α: 90%, E_a: 95.20 kJ/mol), at 45 °C/min for PBS-Cl (α: 90%, E_a: 97.60 kJ/mol) and at 15 °C/min for PBS-CH_3 (α: 90%, E_a: 97.44 kJ/mol).

When the activation energies of the polymers based on their heating rates were examined by keeping their transformation percentages constant, as opposed to the case for their monomers, it was seen that there was a reduction in their activation energies at some transformation percentages. This situation was observed especially in

Table 6 Activation energies and pre-exponential factors of BS-OH calculated from isoconversional method (Flynn–Wall–Ozawa) at 5, 15 and 45 °C/min

α	β_5			β_{15}			β_{45}		
	Tα	Ea (kJ/mol)	A(s^{-1})	Tα	Ea (kJ/mol)	A(s^{-1})	Tα	Ea (kJ/mol)	A(s^{-1})
0.1	401	33.28	4.43×10^{5}	428	35.52	4.15×10^{5}	445	36.93	3.99×10^{5}
0.2	424	35.19	2.78×10^{6}	447	37.10	2.63×10^{6}	465	38.59	2.53×10^{6}
0.3	450	37.35	3.31×10^{5}	492	40.83	3.03×10^{5}	492	40.83	3.03×10^{5}
0.4	522	43.32	3.03×10^{3}	646	53.61	2.45×10^{3}	652	54.11	2.42×10^{3}
0.5	609	50.54	4.33×10^{5}	681	56.52	3.87×10^{5}	701	58.18	3.76×10^{5}
0.6	655	54.36	2.76×10^{8}	696	57.76	2.60×10^{8}	721	59.84	2.51×10^{8}
0.7	677	56.19	8.31×10^{8}	723	60.00	7.78×10^{8}	738	61.25	7.62×10^{8}
0.8	892	74.03	3.24×10^{6}	903	74.94	3.20×10^{6}	799	66.31	3.62×10^{6}
0.9	1113	92.37	3.67×10^{17}	1100	91.30	3.72×10^{17}	1059	87.89	3.86×10^{17}

Table 7 Activation energies and pre-exponential factors of BS-Cl calculated from isoconversional method (Flynn–Wall–Ozawa) at 5, 15 and 45 °C/min

α	β_5			β_{15}			β_{45}		
	Tα	Ea (kJ/mol)	$A(s^{-1})$	Tα	Ea (kJ/mol)	$A(s^{-1})$	Tα	Ea (kJ/mol)	$A(s^{-1})$
0.1	429	35.60	6.70×10^{8}	369	30.62	7.79×10^{8}	447	37.10	6.43×10^{8}
0.2	457	37.93	1.02×10^{8}	460	38.18	1.01×10^{8}	486	40.33	9.63×10^{7}
0.3	536	44.48	1.32×10^{5}	488	40.50	1.45×10^{5}	554	45.98	1.27×10^{5}
0.4	596	49.46	7.28×10^{8}	591	49.05	7.34×10^{8}	628	52.12	6.91×10^{8}
0.5	635	52.70	4.63×10^{8}	650	53.95	4.53×10^{8}	676	56.10	4.35×10^{8}
0.6	667	55.36	8.45×10^{11}	682	56.60	8.27×10^{11}	701	58.18	8.04×10^{11}
0.7	922	76.52	3.85×10^{9}	713	59.17	4.98×10^{9}	723	60.00	4.91×10^{9}
0.8	1024	84.99	1.04×10^{7}	887	73.62	1.20×10^{7}	912	75.69	1.17×10^{6}
0.9	1099	91.21	4.04×10^{9}	1066	88.47	4.17×10^{9}	1123	93.20	3.95×10^{9}

Table 8 Activation energies and pre-exponential factors of BS-CH_3 calculated from isoconversional method (Flynn–Wall–Ozawa) at 5, 15 and 45 °C/min

α	β_5			β_{15}			β_{45}		
	Tα	Ea (kJ/mol)	$A(s^{-1})$	Tα	Ea (kJ/mol)	$A(s^{-1})$	Tα	Ea (kJ/mol)	$A(s^{-1})$
0.1	477	39.59	9.76×10^{9}	487	40.42	9.56×10^{9}	505	41.91	9.22×10^{9}
0.2	492	40.83	2.30×10^{10}	501	41.58	2.26×10^{10}	520	43.16	2.17×10^{10}
0.3	545	45.23	2.08×10^{9}	511	42.41	2.22×10^{9}	536	44.48	2.12×10^{9}
0.4	752	62.41	5.01×10^{5}	549	45.56	6.86×10^{5}	567	47.06	6.64×10^{5}
0.5	839	69.63	7.23×10^{9}	726	60.25	8.36×10^{9}	759	62.99	7.99×10^{9}
0.6	903	74.94	1.15×10^{6}	810	67.23	1.28×10^{6}	844	70.05	1.23×10^{6}
0.7	956	79.34	6.10×10^{6}	887	73.62	6.57×10^{6}	924	76.69	6.31×10^{6}
0.8	1011	83.91	3.76×10^{10}	990	82.17	3.84×10^{10}	1020	84.66	3.73×10^{10}
0.9	1077	89.39	2.69×10^{14}	1129	93.70	2.56×10^{14}	1144	94.95	2.53×10^{14}

Table 9 Activation energies and pre-exponential factors of PBS-OH calculated from isoconversional method (Flynn–Wall–Ozawa) at 5, 15 and 45 °C/min

α	β_5			β_{15}			β_{45}		
	Tα	Ea (kJ/mol)	$A(s^{-1})$	Tα	Ea (kJ/mol)	$A(s^{-1})$	Tα	Ea (kJ/mol)	$A(s^{-1})$
0.1	450	37.35	1.96×10^{5}	432	35.85	2.04×10^{5}	402	33.36	2.20×10^{5}
0.2	527	43.74	2.45×10^{11}	512	42.49	2.48×10^{11}	509	42.24	2.49×10^{11}
0.3	611	50.71	3.65×10^{7}	569	47.22	3.92×10^{7}	575	47.72	3.88×10^{7}
0.4	713	59.17	6.69×10^{5}	636	52.78	7.50×10^{5}	629	52.20	7.58×10^{5}
0.5	804	66.73	8.16×10^{5}	715	59.34	9.1710^{5}	691	57.35	9.49×10^{5}
0.6	892	74.03	4.66×10^{6}	812	67.39	5.12×10^{6}	765	63.49	5.43×10^{6}
0.7	978	81.17	5.26×10^{7}	916	76.02	5.62×10^{7}	849	70.46	6.06×10^{7}
0.8	1059	87.89	5.32×10^{8}	1020	84.66	5.52×10^{8}	964	80.01	5.84×10^{8}
0.9	1159	96.19	3.37×10^{11}	1147	95.20	3.41×10^{11}	1080	89.64	3.62×10^{11}

Table 10 Activation energies and pre-exponential factors of PBS-Cl calculated from isoconversional method (Flynn–Wall–Ozawa) at 5, 15 and 45 °C/min

α	β_5			β_{15}			β_{45}		
	Tα	Ea (kJ/mol)	$A(s^{-1})$	Tα	Ea (kJ/mol)	$A(s^{-1})$	Tα	Ea (kJ/mol)	$A(s^{-1})$
0.1	340	28.22	3.64×10^{6}	353	29.29	3.50×10^{6}	366	30.37	3.38×10^{6}
0.2	448	37.18	1.15×10^{7}	471	39.09	1.09×10^{7}	488	40.50	1.05×10^{7}
0.3	532	44.15	1.19×10^{5}	597	49.55	1.06×10^{5}	584	48.47	1.09×10^{5}
0.4	635	52.70	6.97×10^{5}	713	59.17	6.21×10^{5}	709	58.84	6.24×10^{5}
0.5	710	58.93	4.20×10^{5}	809	67.14	3.69×10^{5}	835	69.30	3.57×10^{5}
0.6	774	64.24	1.50×10^{5}	905	75.11	1.28×10^{5}	950	78.85	1.22×10^{5}
0.7	836	69.38	1.61×10^{5}	988	82.00	1.36×10^{5}	1041	86.40	1.29×10^{5}
0.8	914	75.86	9.86×10^{5}	1062	88.14	8.49×10^{5}	1111	92.21	8.11×10^{5}
0.9	1055	87.56	2.02×10^{8}	1124	93.29	1.89×10^{8}	1176	97.60	1.81×10^{8}

Table 11 Activation energies and pre-exponential factors of PBS-CH_3 calculated from isoconversional method (Flynn–Wall–Ozawa) at 5, 15 and 45 °C/min

α	β_5			β_{15}			β_{45}		
	Tα	Ea (kJ/mol)	$A(s^{-1})$	Tα	Ea (kJ/mol)	$A(s^{-1})$	Tα	Ea (kJ/mol)	$A(s^{-1})$
0.1	448	37.18	2.64×10^{16}	452	37.51	2.62×10^{16}	459	38.09	2.58×10^{16}
0.2	550	45.65	4.01×10^{9}	532	44.15	4.14×10^{9}	526	43.65	4.19×10^{9}
0.3	654	54.28	1.60×10^{8}	623	51.70	1.68×10^{8}	596	49.46	1.76×10^{8}
0.4	758	62.91	2.13×10^{6}	720	59.76	2.24×10^{6}	659	54.69	2.45×10^{6}
0.5	818	67.89	2.58×10^{6}	813	67.47	2.59×10^{6}	725	60.17	2.91×10^{6}
0.6	875	72.62	1.13×10^{7}	896	74.36	1.10×10^{7}	806	66.89	1.22×10^{7}
0.7	936	77.68	3.16×10^{6}	980	81.34	3.02×10^{6}	902	74.86	3.28×10^{6}
0.8	996	82.66	2.35×10^{3}	1066	88.47	2.20×10^{3}	1003	83.24	2.34×10^{3}
0.9	1068	88.64	2.07×10^{6}	1174	97.44	1.88×10^{6}	1111	92.21	1.99×10^{6}

all transformation percentages in the PBS-OH polymer. As the heating rate increased from 5 to 45 °C/min, the activation energy decreased (α: 90%, at 5 °C/min E_a: 66.73 kJ/mol; at 15 °C/min E_a: 59.34 kJ/mol; at 45 °C/min E_a: 57.35 kJ/mol).

In PBS-Cl, a similar result was observed when the transformation percentage became 0.3 and 0.4. The activation energy found at the heating rate of 15 °C/min was higher than those at both 5 °C/min and 45 °C/min (α: 30%, at 5 °C/min E_a: 44.15 kJ/mol; at 15 °C/min E_a: 49.55 kJ/mol; at 45 °C/min E_a: 48.47 kJ/mol). In difference to the other two polymers, in the PBS-CH_3 polymer, activation energies that were not in direct proportion to the transformation percentage and heating rate were obtained. The activation energy increased along with the increasing heating rate when the transformation percentage was 10%, but it decreased when the transformation percentage was 20%, 30%, 40% and 50%. In the interval where the transformation percentage between was 60% and 90%, the activation energy obtained at the heating rate of 15 °C/min was higher than those obtained at 5 and 45 °C/min (α:0.8, at 5 °C/min E_a:82.66 kJ/mol; at 15 °C/min E_a:88.47 kJ/mol; at 45 °C/min E_a:83.24 kJ/mol).

The most important reason for the changes in the activation energies of the polymers was the changes created in the chain structures of the polymers as the ambient temperature increased. Atoms found in the chains in the amorphous or crystalline regions of polymers below the glass transition temperature continue their atom movements that are also valid for small molecules such as translation, vibration and shear. However, the polymer chains cannot perform movements like bending and curving below the glass transition temperature. Therefore, they cannot change their shape or position inside the structure under external forces, and their covalent bonds break when forced excessively.

When the glass transition temperature is reached, the energy required for the chains in amorphous regions to turn around chemical bonds is provided, and the polymer chains can perform bending and curving movements.

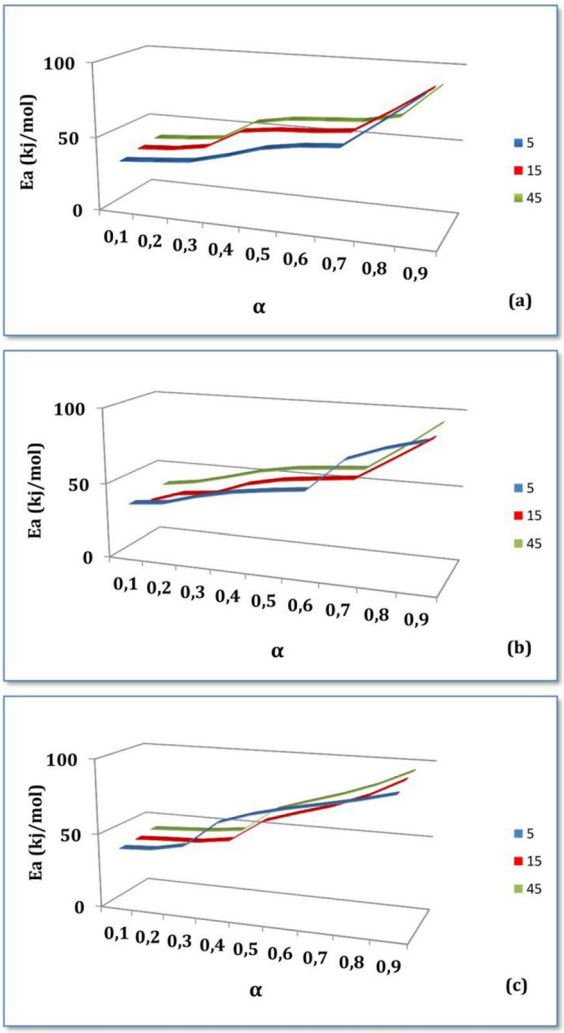

Fig. 24 The activation energy (E_a) of compounds changes with α (**a** BS-OH, **b** BS-Cl, **c** BS-CH_3)

That is, throughout the thermal analysis above TGA that was conducted, the polymers used a part of the energy taken from the outside to undergo their movements, while they used another part of this energy for decomposition. Additionally, as a result of the increased energy, the decomposed polymer units created new structures by recombination.

Calculation of thermodynamic parameters

During all types of movements and chemical reactions, energy absorption, energy release or conversion of one type of energy into another is possible. Examination of the relationships between the different energy types within a system constitutes the subject of thermodynamics. Thermodynamics determines the internal energy, enthalpy, entropy and free energy values of the system during a physical or chemical transformation and examines the dependability of these on the reaction conditions. The following equations were used to examine the changes that occurred in the thermodynamic parameters during the thermal decomposition analyses of the synthesized Schiff base monomers and polymers at the different heating rates [36].

$$\Delta H = E - RT_m \tag{8}$$

$$\Delta G = \Delta H - \Delta ST_m \tag{9}$$

$$\Delta S = 2.303\mathrm{R}\left(Log\frac{Ah}{kT_m}\right) \tag{10}$$

where T_m is the DTA peak temperature, h is the Planck's constant, k is the Boltzmann constant, and R is the universal gas constant. The data obtained as a result of the calculations are given in Table 12.

Enthalpy refers to the energy change in a constant-pressure environment. The heat given to the constant-pressure system is expended not only for the increase in the internal energy but also for the work done against the environment. As enthalpy is a state function, it is

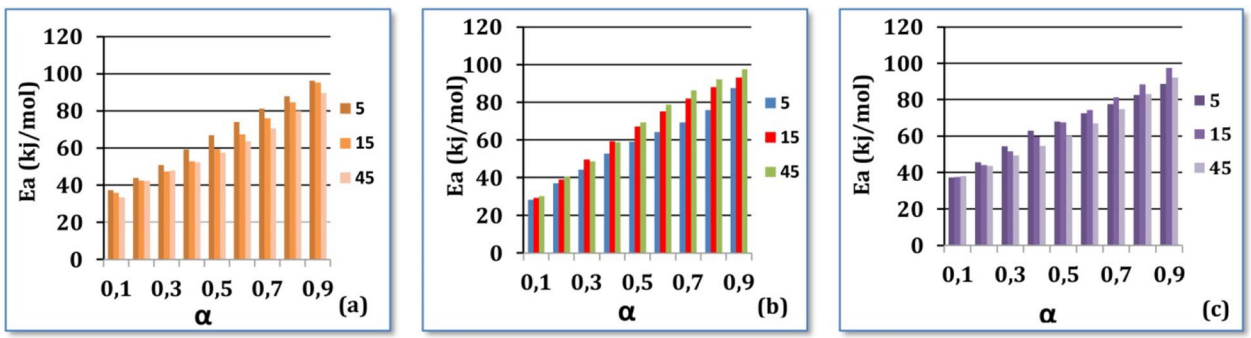

Fig. 25 Changes in the activation energy (E_a) of the polymer compounds with α (**a** PBS-OH, **b** PBS-Cl, **c** PBS-CH_3) at the three heating rate

Table 12 Degradation kinetic parameters for Schiff base compounds at 5, 15 and 45 °C/min, determine by Ozawa method

Compound	Step	β_5			β_{15}			β_{45}		
		ΔH^a	$-\Delta S^b$	ΔG^c	ΔH^a	$-\Delta S^b$	ΔG^c	ΔH^a	$-\Delta S^b$	ΔG^c
BS-OH	1st	149.15	143×10^{-2}	842	113.46	144×10^{-2}	833	116.36	144×10^{-2}	865
	2nd	327.51	129×10^{-2}	1536	394.16	82.8×10^{-2}	1046	387.61	128×10^{-2}	1508
BS-Cl	1st	35.60	79.2×10^{-2}	383	109.31	95.2×10^{-2}	545	123.42	95.9×10^{-2}	574
	2nd	202.02	87.5×10^{-2}	719	218.78	85.8×10^{-2}	778	226.42	86.4×10^{-2}	812
	3rd	252.73	120×10^{-2}	1429	162.09	71.4×10^{-2}	923	168.90	71.9×10^{-2}	937
BS-CH_3	1st	39.59	56.5×10^{-2}	275	82.00	57.1×10^{-2}	333	129.56	57.7×10^{-2}	390
	2nd	148.48	72.5×10^{-2}	591	148.23	61.8×10^{-2}	564	110.05	62.4×10^{-2}	544
	3rd	397.23	94.1×10^{-2}	1403	316.72	62.7×10^{-2}	784	326.35	63.1×10^{-2}	805
PBS-OH	1st	131,80	31.8×10^{-2}	298	237.71	146×10^{-2}	845	296.39	104×10^{-2}	873
	2nd	465.21	69.1×10^{-2}	1093	323.28	106×10^{-2}	1335	240.11	86.9×10^{-2}	1078
PBS-Cl	1st	354.82	139×10^{-2}	1263	244.26	154×10^{-2}	1132	247.50	156×10^{-2}	1651
	2nd	163.42	96.3×10^{-2}	1168	338.55	141×10^{-2}	1827	355.07	157×10^{-2}	2028
PBS-CH_3	1st	267.92	66.1×10^{-2}	629	260.62	66.2×10^{-2}	636	312.99	92.8×10^{-2}	864
	2nd	321.62	134×10^{-2}	1708	341.62	130×10^{-2}	1622	250.32	129×10^{-2}	1487

[a,c] $kJmol^{-1}$; [b] $Jmol^{-1}\ K^{-1}$

path-independent and an exact differential function. The enthalpy function is not dependent on the changing order of the variables (T, P), but it is only dependent on their initial and final states. The enthalpy change between two states is shown as ΔH in Table 12. Considering the enthalpy changes of the monomers and polymers during thermal decomposition, it was seen that their enthalpies decreased in direct proportion to the temperature increase. The highest enthalpy value among the monomers was in the third step of the thermal analysis of the BS-CH_3 monomer conducted at the heating rate of 5 °C/min (ΔH: 397.23 kJ/mol).

The lowest enthalpy value was in the first step of the thermal analysis of BS-Cl conducted at 5 °C/min (ΔH: 35.60 kJ/mol). As in the case of the monomers, there were changes in the enthalpy values of the polymers based on the heating rate. The highest (at 5 °C/min heating rate, ΔH: 465.21 kJ/mol) and lowest (at 5 °C/min heating rate, ΔH: 131.80 kJ/mol) enthalpy values belonged to PBS-OH. Entropy is expressed as the disorderliness of a system, and it is known that a certain energy is spent for a change in entropy. What change system at a certain pressure, a certain temperature and with a certain composition has a single entropy value. The entropy change between two states is shown as ΔS, and entropy change also has a single value. Entropy change is dependent on the heat (q) and temperature (T) values. Thermal degradation reactions enhance the disorder of a system as they are facilitated by providing heat to the system from the outside [27]. The negative ΔS values that were calculated showed (Table 12) that the resistance of the bonds in all monomers and polymers, except for the BS-OH monomer, against thermal decomposition was higher in the first step than the other steps at all heating rates. The highest and lowest entropy values were found among the monomers in, respectively, BS-CH_3 (at 5 °C/min heating rate, ΔS: 56.5×10^{-2} kJ/mol) and BS-OH (at 45 °C/min heating rate, ΔS: 144×10^{-2} kJ/mol). Among the polymers, these values belonged, respectively, to PBS-OH (at 5 °C/min heating rate, ΔS: 31.8×10^{-2} kJ/mol) and PBS-CH_3 (at 45 °C/min heating rate, ΔS: 156×10^{-2} kJ/mol). The opposite of events where entropy decreases while enthalpy increases is spontaneous. In events where both enthalpy and entropy change, the tendency of spontaneity is determined by the enthalpy, entropy and absolute temperature. Depending on this, the entropy may be positive, negative or zero. As a result, events where the enthalpy goes towards the minimum, and the entropy goes to the maximum determine ΔG as a measure of the increase in the tendency of spontaneity (irreversibility). The free energy changes (ΔG) of the thermal decomposition steps of the monomers and polymers were positive. This result showed that the decomposition reactions were irreversible. The highest ΔG value occurred in BS-OH among the monomers (at 5 °C/min heating rate, ΔG: 1536 kJ/mol) and PBS-CH_3 among the polymers (at 5 °C/min heating rate, ΔG: 1708 kJ/mol) in the second step. The lowest ΔG value occurred in BS-CH_3 among the monomers (at 5 °C/min heating rate, ΔG: 275 kJ/mol) and PBS-OH among the polymers (at 5 °C/min heating rate, ΔG: 298 kJ/mol) in the first step. The differences in the free energy changes

show that the steps in the decomposition reactions carry out specific decompositions.

Conclusions

Three novel Schiff base monomers containing boron and three novel polymers by using these monomers as the basic materials were synthesized. There was boron in the aromatic structures of the synthesized compounds. The reason for using boron compounds in the basic materials was that the resistance of boron against heat is high, and it was expected that the boron would transfer this property to the synthesized compounds. For the characterization of the synthesized monomers and polymers, eight different analysis methods were used. The obtained data proved the synthesizability of the designed compounds. TGA/DTA/DTG analyses of the synthesized compounds were carried out at the heating rates of 5, 15 and 45 °C/min. This way, the resistance of the monomers and polymers against heat at different heating rates was investigated. As a result of the TGA analyses conducted in the interval of 20 to 1000 °C, a substantial amount of substances remained undecomposed in both the monomers and polymers. Organic compounds mostly decompose completely at temperatures over 600 °C. The reason for there being substantial amounts of substances remaining in the environment as a result of the thermal analysis was the element boron in the structures of the compounds. The Flynn–Wall–Ozawa method was used to find the thermodynamic parameters of the compounds. When the ΔH, ΔS and ΔG data of the compounds were examined, the highest ΔH values were in BS-CH_3 among the monomers and in PBS-OH among the polymers. The total ΔH values in all three polymers were higher than those of their monomers. The negative ΔS and positive ΔG values of the compounds showed that the compounds had high resistance against heat, and their decomposition reactions were irreversible. The data showed that the entropy values of the polymers were higher than those of the monomers. This was an indication that the thermal decomposition of the polymers occurred more slowly than that of the monomers. Consequently, although the main structures of the monomers were similar, the fact that the groups connected to the structures were different led the compounds to have different thermal stability values. As a result of polymerization, the thermal stability property of the monomers was transferred to the polymers, and as a result of the increase of molecules decrease when polymerized, their resistance of against heat increased. When the ΔH, ΔS and ΔG values of the polymers were compared, the best thermal stability ranking was PBS-OH > PBS-CH_3 > PBS-Cl. Thermal degradation analyzes performed at different heating rates proved that the thermal stability of the Schiff base polymers were higher than that of the Schiff base monomers, especially at high temperatures. This result shows that our newly synthesized Schiff base polymers could be used for thermal insulation, especially in new generation electronic devices.

Acknowledgements
Not applicable.

Author contributions
Dilek Çanakçı carried out all synthesis stages, Dilek Çanakçı carried out writing and review of the manuscript.

Funding
Not applicable.

Availability of data and materials
No datasets were generated or analysed during the current study.

Declarations

Ethics approval and consent to participate
Not applicable.

Consent for publication
Not applicable.

Competing interests
The authors declare no competing interests.

Received: 14 May 2024 Accepted: 7 August 2024
Published online: 13 August 2024

References

1. Miri R, Razzaghiasl N, Mohammadi MK. QM study and conformational analysis of an isatin Schiff base as a potential cytotoxic agent. J Mol Model. 2013;19:727–35. https://doi.org/10.1007/s00894-012-1586-x.
2. Ali SMM, Abul Kalam Azad M, Jesmin M, Ahsan S, Rahman MM, Khanam JA, Islam MN, Shahriar SMS. In vivo anticancer activity of Vanillin semicarbazone. Asian Pac J Trop Biomed. 2012;2:438–42. https://doi.org/10.1016/S2221-1691(12)60072-0.
3. Mounika K, Anupama B, Pragathi J, Gyanakumari C. Synthesis, characterization and biological activity of a Schiff base derived from 3-ethoxy salicylaldehyde and 2-amino benzoic acid and its transition metal complexes. J Sci Res. 2010;2:513–24. https://doi.org/10.3329/jsr.v2i3.4899.
4. Venkatesh P. Synthesis, characterization and antimicrobial activity of various schiff bases complexes of Zn(II) and Cu(II) ions. Asian J Phar Health Sci. 2011;1:8–11. https://doi.org/10.1016/j.rechem.2019.100006.
5. Wei D, Li N, Lu G, Yao K. Synthesis, catalytic and biological activity of novel dinuclear copper complex with Schiff base. Sci China Ser B-Chem. 2006;49:225–9. https://doi.org/10.1007/s11426-006-0225-8.
6. Sondhi SM, Singh N, Kumar A, Lozach O, Meijer L. Synthesis, anti-inflammatory, analgesic and kinase (CDK-1, CDK-5 and GSK-3) inhibition activity evaluation of benzimidazole/benzoxazole derivatives and some Schiff's bases. Bioorg Med Chem. 2006;14:3758–65. https://doi.org/10.1016/j.bmc.2006.01.05.
7. Pandey A, Dewangan D, Verma S, Mishra A, Dubey RD. Synthesis of schiff bases of 2-amino-5-aryl-1,3,4-thiadiazole and its analgesic, anti-inflammatory, anti-bacterial and antitubercular activity. Int J ChemTech Res. 2011;3:178–84. https://doi.org/10.1155/2012/145028.
8. Chandramouli C, Shivanand MR, Nayanbhai TB, Bheemachari B, Udupi RH. Synthesis and biological screening of certain new triazole schiff bases and their derivatives bearing substituted benzothiazole moiety. J Chem Pharm Res. 2012;4:1151–9.

9. Chinnasamy RP, Sundararajan R, Govindaraj S. Synthesis, characterization, and analgesic activity of novel schiff base of isatin derivatives. J Adv Pharm Tech Res. 2010;1:342–7. https://doi.org/10.4103/0110-5558.72428.
10. Sathe BS, Jaychandran E, Jagtap VA, Sreenivasa GM. Synthesis characterization and anti inflammatory evaluation of new fluorobenzothiazole schiff's bases. Int J Pharm Res Develop. 2011;3:164–9. https://doi.org/10.1155/2013/893512.
11. Chaubey AK, Pandeya SN. Synthesis & anticonvulsant activity (Chemo Shock) of Schiff and Mannich bases of Isatin derivatives with 2-Amino pyridine (mechanism of action). Int J PharmTech Res. 2012;4:590–8. https://doi.org/10.1016/s0014-827x(99)00075-0.
12. Aboul-Fadl T, Mohammed FA, Hassan EA. Synthesis, antitubercular activity and pharmacokinetic studies of some Schiff bases derived from 1-alkylisatin and isonicotinic acid hydrazide (INH). Arch Pharm Res. 2003;26:778–84. https://doi.org/10.1007/BF02980020.
13. Avaji PG, Vinod Kumar CH, Patil SA, Shivananda KN, Nagaraju C. Synthesis, spectral characterization, in-vitro microbiological evaluation and cytotoxic activities of novel macrocyclic bis hydrazone. Eur J Med Chem. 2009;44:3552–9. https://doi.org/10.1016/j.ejmech.2009.03.032.
14. Dhar DN, Taploo CL. Schiff bases and their applications. J Sci Ind Res. 1982;41:501–6.
15. Tian LT, Yuan ZL, Long YZ, Chi MX, Sa D. Synthesis of boronic acid-functionalized soluble dendrimers and its application in detection of human liver microsomal glycoprotein based on enzyme-linked ımmunosorbent assay, Chin. J Anal Chem. 2017;45:1259–63. https://doi.org/10.1039/C5AY02131F.
16. Li FL, Zhao X, Xu G. Synthesis and application of a nitrobenzeneboronic acid-substituated silica for affinity chromatography. Chin J Anal Chem. 2006;34:1366–70. https://doi.org/10.1016/j.aca.2006.07.058.
17. Song-Jie H, Ming-Yuan L, Jun J, Ying W, Chang H, Yun-Jie B, Yang T. Determination of new halogenated flame retardants in human serum by gel permeation chromatography-gas chromatography-mass spectrometry. Chin J Anal Chem. 2012;40:1519–23. https://doi.org/10.1016/s1872-2040(11)60578-1.
18. Chou J, Zhang Y, Lu HJ, Yang PY. Small size 4-mercaptophenylboronic acid functionalized gold nanoparticles for selective enrichment and mass spectrometric ıdentification of glycoproteins in rat liver. Acta Chim Sinica. 2011;69:2123–9. https://doi.org/10.1002/rcm.4258.
19. Pan MR, Sun YF, Zheng J, Yang WL. Boronic acid-functionalized core-shell-shell magnetic composite microspheres for the selective enrichment of glycoprotein. ACS Appl Mater Interfaces. 2013;5:8351–8. https://doi.org/10.1021/am401285x.
20. Wang H, Bie Z, Lü C, Liu Z. Magnetic nanoparticles with dendrimer-assisted boronate avidity for the selective enrichment of trace glycoproteins. Chem Sci. 2013;4:4298–303. https://doi.org/10.1039/C3SC51623G.
21. Xu YW, Wu ZX, Zhang LJ, Lu HJ, Yang PY, Webley PA, Zhao DY. Highly specific enrichment of glycopeptides using boronic acid-functionalized mesoporous silica. Anal Chem. 2009;81:503–8. https://doi.org/10.1021/ac801912t.
22. Liu L, Zhang Y, Zhang L, Yan G, Yao J, Yang P, Lu H. Highly specific revelation of rat serum glycopeptidome by boronic acid-functionalized mesoporous silica. Anal Chim Acta. 2012;753:64–72. https://doi.org/10.1016/j.aca.2012.10.002.
23. Zhang Y, Yang JN, Nie JF, Yang JH, Gao D, Zhang L, Li JP. Enhanced ELISA using a handheld pH meter and enzyme-coated microparticles for the portable, sensitive detection of proteins. Chem Commun. 2016;52:3474–7. https://doi.org/10.1039/c5cc09852a.
24. Bi X, Liu Z. Enzyme activity assay of glycoprotein enzymes based on a boronate affinity molecularly ımprinted 96-well microplate. Anal Chem. 2014;86:959–66. https://doi.org/10.1021/ac503778w.
25. Çanakçı D. Synthesis, spectroscopic, thermodynamics and kinetics analysis study of novel polymers containing various azo chromophore. Sci Rep. 2020;10:477. https://doi.org/10.1038/s41598-019-57264-3.
26. Pandy JH, Ganatra KJ. Synthesis, characterization and biological evaluation of bis-bidentate Schiff base metal complexes. Inorg Chem Indian J. 2008;3:182–7.
27. Joshi KR, Rojivadiya AJ, Pandya JH. Synthesis and spectroscopic and antimicrobial studies of Schiff base metal complexes derived from 2-Hydroxy-3-methoxy-5-nitrobenzaldehyde. Int J Inorg Chem. 2014;2014:1–8. https://doi.org/10.1155/2014/817412.
28. Al-Karkhi IHT, Yaseen AK, Shamkhy ET. Synthesis, characterization bioactivity and cytotoxicity of NS Schiff base and its Ni(II), Cd(II) and Zn(II) metal complexes. J Thi-Qar Sci. 2014;4:52–8. https://doi.org/10.32792/utq/utjsci/vol4/2/7.
29. Osypiuk D, Cristóvão B, Bartyzel A. New coordination compounds of Cu(II) with Schiff Base ligands—crystal structure, thermal, and spectral ınvestigations. Crystals. 2020;10:1004. https://doi.org/10.3390/cryst10111004.
30. Nazirkar B, Mandewale M, Yamgar R. Synthesis, characterization and antibacterial activity of Cu (II) and Zn (II) complexes of 5-aminobenzofuran-2-carboxylate Schiff base ligands. J Taıbah Unıv Scı. 2019;13:440–9. https://doi.org/10.1080/16583655.2019.1592316.
31. Thamaraikannan T, Jayalakshmi R, Muthusami R, Akila E, Rajavel R. Exploration of new mononuclear Schiff Base Cu (II), Ni (II) and Co (II) complexes using physicochemical methods. IOSR J Appl Chem. 2017;10:46–53. https://doi.org/10.9790/5736-1008014653.
32. Fritsch L, Merlo AA. An old dog with new tricks: Schiff bases for liquid crystals materials based on isoxazolines and isoxazoles. Chemistry. 2016;1:23–9. https://doi.org/10.1002/slct.201500044.
33. Çanakçı D. Thermal stability, degradation kinetic and structural characterization of novel aromatic amide compounds. J Mol Struc. 2020;1205:127645. https://doi.org/10.1016/j.molstruc.2019.127645.
34. Flynn JH, Wall LA, Quick A. Direct method for the determination of activation energy from thermogravimetric data. Polym Lett. 1966;4:323–8. https://doi.org/10.1002/pol.1966.110040504.
35. Takeo O. A new method of analyzing thermogravimetric data. Bull Chem Soc Jpn. 1965;38:1881–6. https://doi.org/10.1246/bcsj.38.1881.
36. Humienik MO, Mozejko J. Thermodynamic functions of activated complexes created in thermal decomposition processes of sulphates. Thermochim Acta. 2000;344:73–9. https://doi.org/10.1016/S0040-6031(99)00329-9.

Publisher's Note